ADDIS ABABA UNIVERSITY

ADDIS ABABA INSTITUTE OF TECHNOLOGY (AAIT)

SCHOOL OF MECHANICAL AND INDUSTRIAL ENGINEERING

DESIGN, MODELING, AND ANALYSIS OF A HAWT WITH A PASSIVELY INDUCED MORPHING BLADE

A THESIS

SUBMITTED IN PARTIAL FULFILMENT OF THE REQUIREMENTS

FOR A MASTER'S DEGREE

IN

MECHANICAL ENGINEERING (THERMAL ENGINEERING)

Amare Adihena

ID: GSE/2064/11

Advisor: Asfaw Beyene, [Ph.D]

Co advisor: Yilma Tadesse [Ph.D]

Addis Ababa, Ethiopia

Acknowledgment

Completing this thesis project could not have been possible without the assistance of many people whose names may not be listed here. Their contributions are gratefully acknowledged.

Frist I would like to give my special thanks to my advisors Professor Asfaw Beyene and Dr. Yilma Tadesse for their eye opening ideas, endless support, at every stage their devotion, clarity, and sharing of their invaluable ideas as well as experience is greatly appreciated.

I would like to say thanks again to all relatives and friends who stood beside me and give critical feedback and many helpful ideas, especially to Ashenafi A. and Tikaw H.

Above all, to the Almighty of God with his mom snit. Merry, the author of knowledge and wisdom for his endless Love and care.

Abstract

Wind energy become a major form of energy in the past decades, which needs extensive research activities to improve power efficiency. Herein, a Palm tree-inspired morphing blade novel concept design is introduced to improve the power efficiency of conventional HAWTs. The rotor speed is regulated by a twist-augmented bending system and the blade restoration at low tip speed is performed by a spring-augmented pivot hinge system. The main objective of this research project is to design, a 3D model, and Analysis of a HAWT with a passively induced morphing blade. A NACA 4412 Applicable profiles is selected for the proposed morphing blade design. A knowledge-based design compatibility analysis (DCA) was investigated, indeed the design is compatible. The 3D model of the proposed morphing blade was done using CERO PTC 8, and ANSYS Fluent 2021R2 was used for the CFD analysis. The computational geometry was discretized in a well-structured fine tetrahedral cell with the recommended skewness <0.95 and orthogonal quality >0.1. The CFD analysis was based on the simplified Reynolds Averaged Navier Stokes (RANS) governing equations with a steady-state Spalart-allmaras turbulence viscous model. From the CFD simulation results, the average power produced at an annual mean wind speed was 870 KW. In addition, the linear relationship between the theoretical (analytical), and CFD simulation results of power coefficient (Cp), Tip speed, and produced power, shows a very strong correlation. To compare the Annual Energy production (AEP), a conventional SANY SE7715 wind turbine installed in the Adama II wind farm project with the same operating conditions and partial design specifications was taken as a reference site. Using the software-based analysis results, the AEP of the newly introduced morphing blade at annual mean wind speed is 7.62 GWh. Likewise, the average AEP of the reference site as per the prior researcher's investigation is 5.59 GWh. which is about 570 GWh gross AEP for the total 102 sets. This indicates the AEP of the novel morphing ability wind turbine design is 36.4 % higher than the reference site. Finally, the detailed design of the inner structures of the palm tree-inspired morphing blade, detailed structural load analysis, prototype, and experimental investigations are part of the future work.

Keywords: Wind, morphing blade, Palm tree, HAWT, 3D modeling, CFD, Compatibility design analysis (DCA), Life cycle analysis (LCA), Efficiency

Table of Contents

List of Figures

List of Tables

Nomenclature

WTG	Wind Turbine Generator
CWT	Conventional wind turbines
MB	Morphing Blade
BA	Bending angle
HAWT	Horizontal-Axis Wind Turbine
VAWT	Vertical-Axis Wind Turbine
FPB	Fixed Pitch Blade
BPC	Blade with Pitch Control
AEP	Annual Energy Production
BEMT	Blade Element Momentum Theory
LDWT	Large Diameter Wind Tunnel
SDSU	San Diego State University's
MPPT	Maximum Power Point Tracking
DPC	direct power control
IPC	Indirect power control
CFD	Computational Fluid dynamics
DCA	Design compatibility Analysis
TSR	Tip speed ratio
MI	Match index
RANS	Reynolds Averaged Naiver Stokes
LCA	Life cycle Analysis
ISO	International Standards Organization
GWh	Giga Watt hour
θ	Bending angle
$A_{cut\text{-}in}$	Swept area at cut-in alignment
A_{rated}	Swept area at rated alignment
A_{stowed}	Swept area at stowed alignment
D	Diameter
r	Cord length of the blade

t	Root length
C_p	Power coefficient of a wind turbine rotor
V	Wind speed
V_{tip}	Tip speed
V_{rated}	Rated speed
p(v)	Probability for the wind speed
ω	Angular speed
F_c	Centrifugal force
F_t	Trust force
F_s	Spring force
F_g	Gravitational force
F_r	Resultant force

Chapter One: Introduction

1.1. Background

Even though Energy Utilization plays a great role in modern civilization, finding a reliable energy resource become one of the major challenges and worthy in today's world. Conventional energy sources such as coal, natural gas, and fossil fuels have enhanced the industrialization and modernization of different nations. However, the global anxiety around the world is the impact of global warming from greenhouse gases emission into the atmosphere as a result of these traditional energy sources. For this reason, renewable and sustainable energy resources are getting global attention as a new dimension to mitigate carbon emissions.

The first historical background of wind energy was found by the Hero of Alexandria in the first century A.D. by introducing a windmill to the world for the first time [9]. The second reference is from Al Masudi's report, which indicates vertical axis windmills called Seitan windmills were used in Persian in the 9th century A.D. [10]. In addition, the first windmills in Europe were installed in the 12th century with four blades as the primary sources of energy. However, after the industrial revolution, these types of windmills disappeared due to their non-dispatch ability and non-transportability [9]. Today according to GWEC's & IRENA 2021 report, the world recorded a global cumulative wind power capacity of 743 GW, which helps to avoid over 1.1 billion tons of CO2 globally [3].

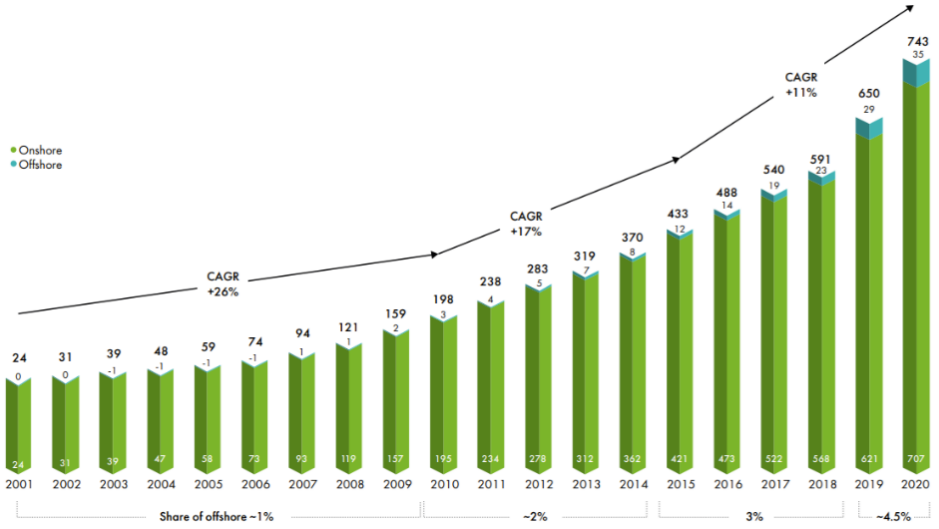

Figure 1: Global cumulative wind power capacity C. Global [3].

According to the modern classification, there are two types of wind turbines, horizontal axis wind turbine (HAWT) and Vertical axis wind turbine (VAWT) and this classification is based on the axis of rotation.

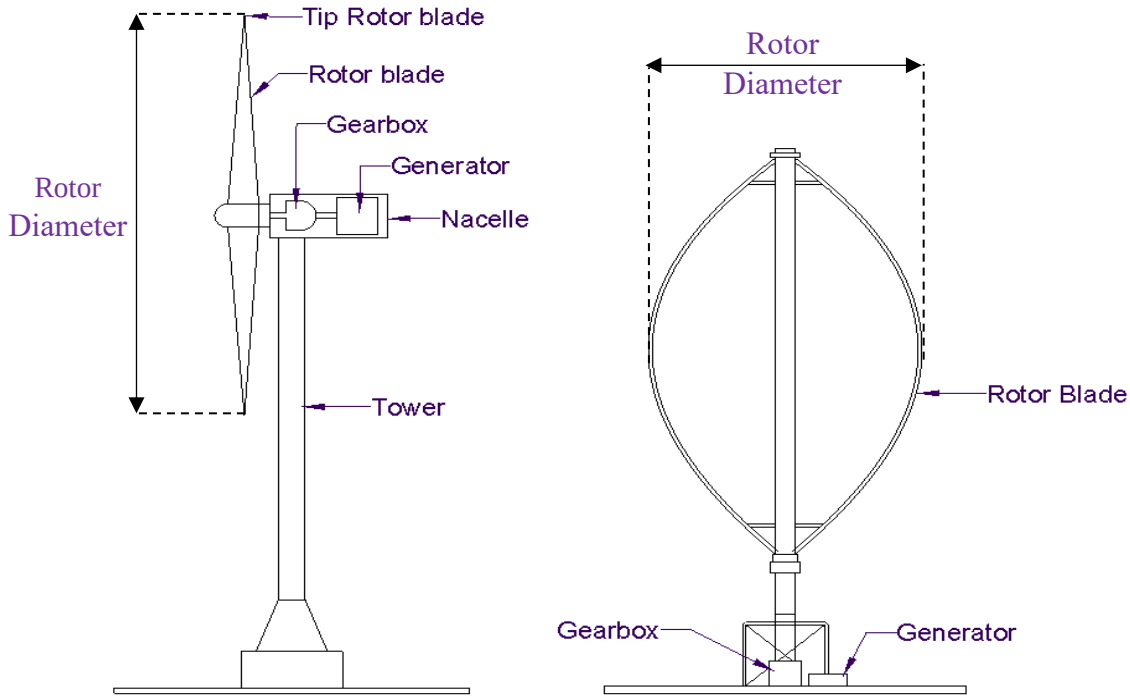

Figure 2: a) Horizontal and b) Vertical Axis Wind Turbine's Configuration.

1.1.1. Conventional wind turbine

Conventional wind turbines have a rigid blade at fixed optimal pitch distribution achieving simultaneously a solid rotation of all the blades of the turbine around their radial hub [11]. The main problem and limitation of the conventional wind turbine blade is its rigid structure, which is not flexible in reaction to wind direction and speed. However, this is the main reason why conventional wind turbines are working under a specific wind speed operating range with low efficiency and a short lifetime. Globally most wind farm projects are rigid blade wind turbines, for example, from IRENA 2021 report, the conventional wind energy capacity installed in Africa is 7.33 GW, in South America, 29.10 GW, in North America 155.13 GW and in Asia 397.27GW [3].

Since vertical axis wind turbines (VAWTs) operate at a less effective drag method, it is not at the performance and efficiency level compared to the HAWT. However, this thesis project focuses on the Performance improvement of HAWT using a passively induced morphing blade.

Figure 3: Adama I wind farm project (conventional wind turbine) A. MUKTAR [1]

Figure 3, is a conventional wind turbine Adama I wind farm project with 51 MW installed capacity located in Ethiopia.

1.1.2. Morphing wind turbine

The main problem and limitation of the conventional wind turbine blade is its rigid structure, which is not flexible in reaction to wind speed. This problem can be solved by introducing new concepts on wind turbine blade profiles, and design techniques. Recently the concept of morphing on wind turbine blades is introduced, which deforms surely in reaction to wind load, and has been derived from fish locomotion, spoilers, and ailerons [12]. Using morphing blade technology, it is possible to improve the performance of wind turbines by up to 20% over conventional wind turbine blades [13]. Depending on the type of twist control morphing blades (MB) can be either “passive” or “active”.

1.1.2.1. Active morphing blade

To achieve the desired twist distribution active morphing blades are made up of several independent span-wise sections [14]. Due to the greater lift coefficient of active morphing blades, greater efficiency is achieved in a wide range of wind speeds and tip speed ratios, but the application of active morphing blades is very limited as a result of its complex structure and high operational cost compared to the passive morphing blade.

1.1.2.2. Passive morphing blade

Passive morphing is a monolithic concept that relies on the elastic deformation of blade structure, which allows the blade to position itself more effectively in varying operational conditions and enables higher efficiency over a wider range of operational conditions [14]. The drag coefficient in passively induced

morphing blades is less than the identical geometry of rigid conventional blades, this allows the passive morphing blade to have higher blade torque and efficiency. We can see a Morphing blade wind turbine from nature inspired by the Palm Tree under wind load as shown in Fig. 4.

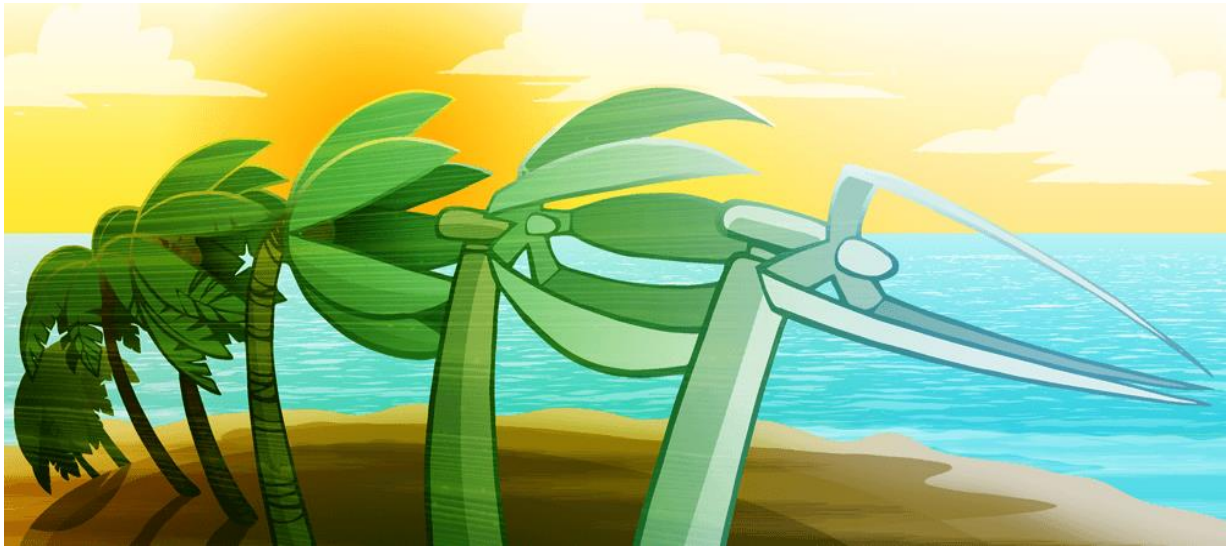

Figure 4: Morphing blade wind turbine inspired by the Palm Tree (Artwork by Kirk Anderson)

This thesis project focus on, Design, modeling, and analysis of a passively induced morphing blade for HAWT. Since vertical axis wind turbines (VAWTs) operate at a less effective drag method, its performance and efficiency level is limited compared to the HAWTs. To address the economic advantage of the newly introduced morphing blade over the conventional installed HAWT projects using Life cycle Comparative analysis with assumed Rayleigh distribution, this paper focuses on performance improvement of HAWTs blades using passivity induced morphing blade. Generally, in this paper, to improve the power efficiency of the HAWT, a flat NACA profile will be selected; morph to give a palm-leaf look, and conduct 3D CFD simulation for a twist augmented bending will be the concept design. The expected advantage of this passively induced morphing blade design for a HAWT is to improve the power efficiency and lifetime of the wind turbine blade.

1.2. Statement of the Problem

Wind energy plays a great role in the current global framework of the green industrial revolution as a new dimension in mitigating carbon emissions. Hence, many researchers are working on extensive research activities to improve the conventional wind turbine drawbacks by introducing innovative ideas. The main problem of the conventional wind turbine is its rigid blade structure, prohibiting the flexibility of the system for the intermittent nature of wind direction and speed. Due to this problem conventional wind turbines (CWTs) are limited to:

1. Very low efficiency usually less than 50% since they work under a specific wind speed range
2. Short lifetime due to induced stresses in the blade during a dangerous wind situation.

Research indicates that wind turbines fail around twice every year with an average downtime of 150 h per failure. The most critical component in terms of downtime is the gearbox as a result of high wind loads [42].

Figure 5: WTG destroyed in Texas as a result of high wind load (by Jeremy Rockit)

According to the latest US Department of Energy and National Renewable Energy Laboratory (NREL), (2009-2015) statistics report, out of 750 confirmed wind turbine gearbox damage records, the majority of wind turbine gearbox failures (76%) are caused by the bearings, as a result of axial cracks in high and intermediate wind speed stages, as a result, some wind projects experience failure rates of up to 50 percent within the space of a few years before the payback period [43].

1.3. Objective

1.3.1. General objective

The general objective of this research project is to design, modeling, and Analysis of a HAWT with a passively induced morphing blade.

1.3.2. Specific objective

The specific objectives are:

1. To conduct previously published peer-reviewed works of literature.
2. To prepare the design parameters of the HAWT morphing blade.
3. Mathematical, Geometrical, and Numerical Modeling of Morphing Blade.
4. To conduct a life cycle assessment-based comparative analysis of annual energy production.

1.4. Scope of the Project

The scope of the project includes the Design, 3-D modeling, and Analysis of a HAWT with a passively induced morphing blade. To study the compatibility between the required design requirements and the proposed morphing blade design a knowledge-based design compatibility analysis (DCA) is considered.

Chapter Two: Literature Review

2.1. Part-Load Issues

Partial load region and full load regions are the two primary regions of wind turbine speed Regimes in well-controlled wind turbine technologies as shown in Fig. 6. The cut-in speed in partial load is the minimum wind speed at which the wind turbine starts to generate usable power and the cut-out speed at the full load is the one at which the pitching system is activated to stop the turbine to avoid any damage due to high wind stress. The partial load region is a region where wind speed varies between cut-in speed and rated speed rated, whereas the full load region is a region where wind speed varies between rated speed rated and cut-out speed. The wind turbine rotor speed is proportional to the wind speed and the torque exerted on the rotor. The wind turbine power transmission system requires a part load to operate very effectively.

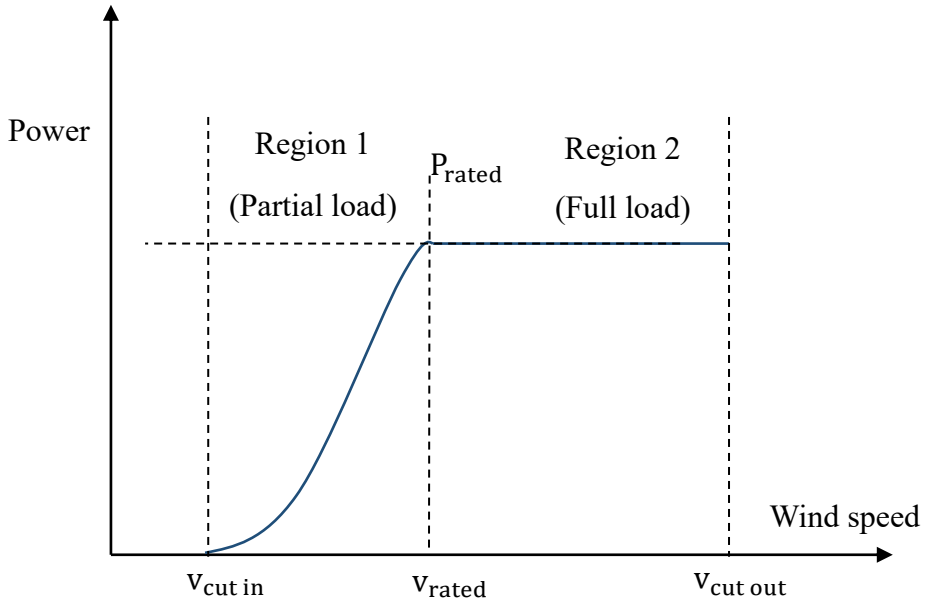

Figure 6: Power operating regions of a wind turbine

2.2. Pitch-control

To improve the power output of wind turbine technology using the available wind energy resources, and its intermittent nature numerous research activities were performed by many scholars. One output of such research activities was introducing the concept of a pitch control mechanism that adjusts the angle of wind turbine rotor blades to get the right fraction of the available wind and maintain the

Safety of the wind turbine at high wind loads and other catastrophic events without exceeding its maximum rotational speed.

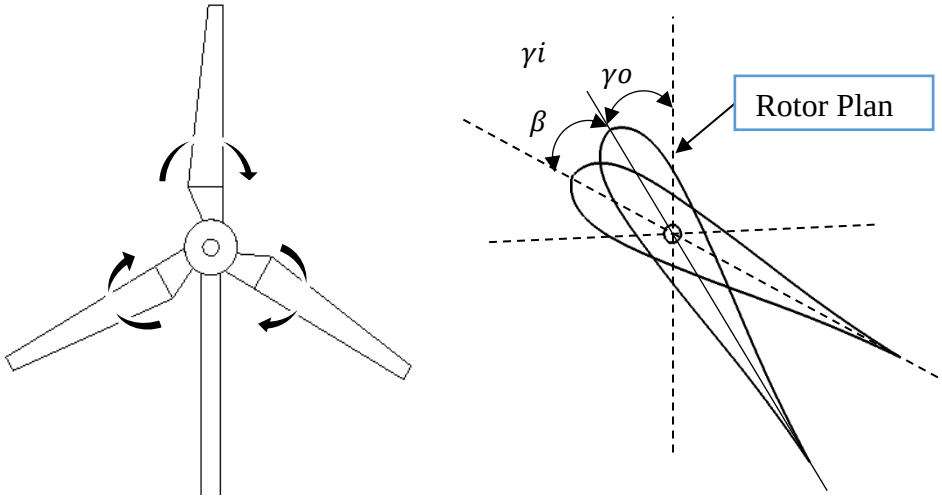

Figure 7: Schematic of the blade with pitch control (BPC)

Any adjustment using the pitch control system does not affect the shape of the blades, but the adjustment will result in all sections which experience the same change in actual twist angle. From the above Fig. 7, the i^{th} element actual twist angle is the sum of the pre-twist angle (γ_o) and the pitch control angle (β).

$$\gamma_i = \gamma_o + \beta$$

According to R. Opie [16], the pitch control mechanism plays a great role in the capital expense which accounts for about 3% less than the conventional rigid-blade wind turbine. But the big challenge of the pitch control system is its subsystem failure during wind turbine downtime, however, this makes it difficult for frequent service and maintenance of the pitch actuator on the wind turbine blade, hence technicians must travel to the remote site and climb more than 260 ft tower during maintenance time.#

2.3. Morphing Blade Mechanism and Techniques

Wind energy is key to the nation's 2030 goals of increased energy independence and reduced environmental impact resulting from power generation [15]. As a result, extensive research activities are encouraged on power improvement of conventional wind turbines by introducing new concepts on wind turbine blade profiles, design techniques, and mechanisms. One method to improve the efficiency is by introducing the morphing blade concept which deforms surely in reaction to wind load. However, recently introduced morphing wind turbine blades have been derived from fish locomotion, spoilers, and ailerons [13]. From this concept design, morphing blade design has been recognized due to its performance

improvement using passive changes in blade geometry. This mechanism is a novel design approach with the ability to optimize the blade profile according to the direction of the wind load. This can be passive or active depending on the blade twist control mechanism. According to some recent research activities, different design techniques have been developed to overcome the blade morphing ability. Herein a detailed literature review is conducted as a case study on published works of morphing ability wind turbine profiles, types, design techniques, and Performance ranges as follows.

A. Rathod et al [13], have developed a morphing concept design using segmented blades connected by screw sockets, and a tension cable system that effectively acts as a passive pitch control for rotor speeds is proposed for future large-scale wind turbine applications. Herein the morphing concept was proposed to accomplish using segmented blades connected by screw sockets and a tension cable system which effectively acts as a passive pitch control for rotor speeds. This proposed concept works at low wind speeds, to ensure maximum power at startup the segmented blades are fully tensioned, and at high rotor speed, to overcome over speed and spine the rotor blade the cable tension proposed to design such that centrifugal forces will drive the blade segments outward. The design of blade segment airfoils was proposed design with a center of pressure downstream of the socket axis to unwind the blade segment at high wind speeds. In addition, the author also considers the design for manufacturability (DFM) of the segmented morphing blade concept which can be easily manufactured and shipped for large-scale applications. In the proposed concepts, the bending loads will be carried by the segmented rotor. Which causes larger downstream deflections of the blades at high wind speeds. Hence, a downstream design would be recommended to avoid the potential strike of the blades with the tower. However, this morphing concept faces several technical challenges, herein the author identifies two major challenging issues which may prevent the morphing segmented concept from becoming a feasible wind turbine concept for extreme-scale applications:

3. At high aerodynamic loading conditions, there will be high spar bending loads in the downwind direction this case to develop high structural stresses on the system.
4. Because of the reduced system stiffness, there will be chord-wise and/or span-wise dynamic instability of the blade elements.

Future works are recommended to focus on the quantitative benefits and disadvantages of the morphing segmented concept using a measurable system-level basis. This will help determine its feasibility and whether detailed simulations and experiments are appropriate.

W. Wang et al. [14], in their work, a simplified morphing blade with a linear twist distribution along the span is introduced to improve the power capture ability of wind turbines. The shape of the morphing blade was controlled by adjusting the twist of the blade's root and the tip. The NREL Phase VI wind turbine blade with a fixed pitch is selected as a reference and based on the blade element momentum theory the performance of the wind blade optimization problems associated with the control of the morphing blade and a blade with pitch control is evaluated and validated. The results show that the morphing blade gives better results than the blade with pitch control in terms of produced power. The other detailed investigation in this paper was the evaluation of annual energy production for three types of blades namely morphing blade, blade with pitch control, and fixed pitch blade. This was done based on a Rayleigh distribution principle under specific assumptions of annual average wind speed given site varying from 5 m/s to 15 m/s and the final evaluated results of the annual energy production of the wind turbine containing morphing blades are (24.5 % - 69.7 %) higher than pitch-fixed blades. The annual energy production of the wind turbine containing pitch control is (22.7 % - 66.9 %) higher than pitch fixed blades. Finally, the researchers suggested that the detailed design of the inner structures of the proposed simplified morphing blade is part of future work.

M. Puterbaugh and A. Beyene [17], in this paper, a detailed parametric relationship between an asymmetric wind turbine blade and constituent material modulus to visualize the geometric response of the morphing blade for a given material characteristic is investigated. Here two different finite element software (VisualFEA, and NASTRAN) were used to verify the trailing edge deflection calculations. And the asymmetric NACA 4412 airfoil with a maximum camber of 0.4c and thickness of 0.12c was selected for the detailed analysis of the parametric relationship. Four different cantilevered beam models of a morphing blade were modeled and the morphing wind turbine blade was subjected to a uniform distribution of three different load cases (partial, rated, and full) wind velocity loads. The result shows as the thickness of varying cross-section are increased and tapered to the trailing edge the modulus value decreases. The concluded results of this research paper show that an airfoil, like a tapered beam, can be modeled as a non-prismatic cantilevered beam using this well-established method, and the Authors maintained that Lab tests can provide further detailed and efficient analysis, however testing a blade of this size and magnitude is beyond the scope of this research paper.

P. Krawczyk et al. [18], in this paper "fluid-structure interaction of a morphed wind Turbine Blade," introduced to achieve continuous morphing to desired and predetermined blade design geometry using CFD and FEM techniques. One of the serious challenges in energy systems design, especially in wind turbines, is the system operation needs to match the variable load because the wind turbine system

efficiency drops with the load design limit. There are many strategies to address part load challenges in wind turbine blades, in this paper varying blade geometry was introduced as a solution to obtain optimum efficiency within the blade design load range. NACA 4412 profile is a common wind turbine blade profile that is used in most applications and is selected to evaluate the aerodynamic behavior of a morphing wind turbine airfoil using a 2-dimensional computation in this paper. In this paper, a 100KW power output 'virtual' wind turbine with a 10 m length, 2 m hub blade dimension, and 7.59 m/s rated wind speed to obtain the required power output was selected for modeling. Generally, the fluid-structure interaction of a chord-wise morphing NACA 4412 airfoil was investigated in 18 cases, which are combinations of six wind velocity regimes and three Young's modulus of blade material, to evaluate aerodynamic forces based on trailing edge deflection, wind speed, elastic property and young's modulus of the material. Finally, the 2-Dimensional computational results show that the morphing blade has greater part-load efficiency than the rigid NACA blade.

D. W. MacPhee and A. Beyene [12], In this work feasibility of morphing blade design passively adapted to local flow conditions to increase power output efficiency for vertical axis wind turbine (VAWT) was investigated. The 'virtual' three-bladed NACA0015 VAWT with a height of 3 m height, c¼0.4 m chord length, and 1.25 m radius of 1.25 m was selected for the detailed investigation of this work. Using OpenFOAM computational fluid dynamics software with the k–ω-SST turbulence model, a rigid VAWT is investigated hence good agreement is found within the existing experimental data. Then the rigid VAWT simulation and experimental results are compared to other geometrically identical VAWT morphing designs by varying material flexibility. From the CFD simulation results, all VAWT morphing blade designs achieved 9.6% higher efficiency than the selected rigid blade design. The CFD simulation result shows the significant advantage of morphing blade design over the rigid blade design, especially in part-load scenarios, and increases the abilities of self-starting for the VAWT. Finally, the detailed analysis of the VAWT morphing and rigid blade design scenario, [12], concluded three points, and put suggestions for further effort to study the impact of the morphing blade over a wider range of tip-speed ratios, material density, and elastic moduli.

i. When compared to identical rigid blade design in part-load scenarios morphing blade design achieves higher efficiency.
ii. The morphing blade performs as a passive pitch control mechanism, unlike a rigid one.
iii. Due to very low (negative) minimal torque morphing the blade helps to reduce the oscillatory structural VAWT loadings.

A. R. Ali et al. [41], this paper investigate the aerodynamic analysis of morphing blade for horizontal axis wind turbine and only the effect of the morphed trailing edge of the wind turbine blade at different blade segment morphing angles of $(0°, 10°, \text{and } 20°)$ is considered for the detail aerodynamic analysis of the morphing blade. The 3-Dimensional CFD analysis of the blade was performed using Star CCM+ computational fluid dynamics software at different morphing blade angles and wind speeds and the results show that power increases as the morphing angle increases. And the blade part was modeled and prototyped with wood material for the wind tunnel testing [20], and the test was carried out at 5 m/s in the wind tunnel test section of (0.35×0.35×0.45) meter dimensions with a maximum attainable speed of 20 m/s. Finally, the wind tunnel testing validates CFD results and proved morphing blade power efficiency increases as the morphing blade angle increases and concluded that morphing wind turbine blade is suitable for all angles and morphing for low wind speed is a safe option.

T. Chuamvarasart et al. [19], in this work, the Conceptual design of wind turbine blades (under 250KW) with morphing ability, is introduced. The major drawback of rigid wind turbine blades is the performance of power production is limited within the range of operation wind speed. This work focused to narrow the limitation of stall control turbines which need continuous performance improvement with a wide range of wind speeds by introducing morphing ability blade design. In this paper, small memory shape actuators were used for the morphing mechanism to enable the morphing capability of the wind turbine blade for the performance improvement of the wind turbine by extending the wind speed operating range. The Author starts the morphing blade design by selecting Clark-Y airfoil profile and memory shape actuator technology as a morphing actuator [21], due to its compact size compared to traditional actuator mechanisms. Based on the Rayleigh distribution principle under specific assumptions of wind speed data, the annual power capacity and power coefficient results of the rigid blade and morphing blade wind turbine have been compared. The results show that;

- The morphing blade WT produces 2172.5 kW·hr/year or 24.8% in annual capacity
- The rigid blade WT annual capacity produces 1728.52 kW·hr/year or 19.73%.

Therefore, as per this work when we compare the morphing ability of wind turbines with the rigid blade bassline there is 444.0 kW·hr./year or 5.07% annual power increment, which is a significant improvement. Finally, the authors suggested that do furthermore work on the actuator mechanism and automatic control system for the working prototype as future work.

D. W. MacPhee and A. Beyene [5], in this paper, geometrically identical rigid and morphing horizontal axis wind turbine blades were examined using both experimental and numerical analysis. Both rigid and flexible blades were built with a simplified approach of symmetric NACA 0015 profiles. The material for both flexible and rigid blades was polyurethane with a density of 1050 kg/m3, and the Hub was printed from ABS material. "Experiments were conducted at the Large Diameter Wind Tunnel (LDWT) 93 laboratory at San Diego State University, which can capable of up to 9.3 m/s wind speed, as shown in Fig. 8 [5]. " The experimental analysis was done with the assumption of low turbulence intensity due to the inlet boundary being open to the environment.

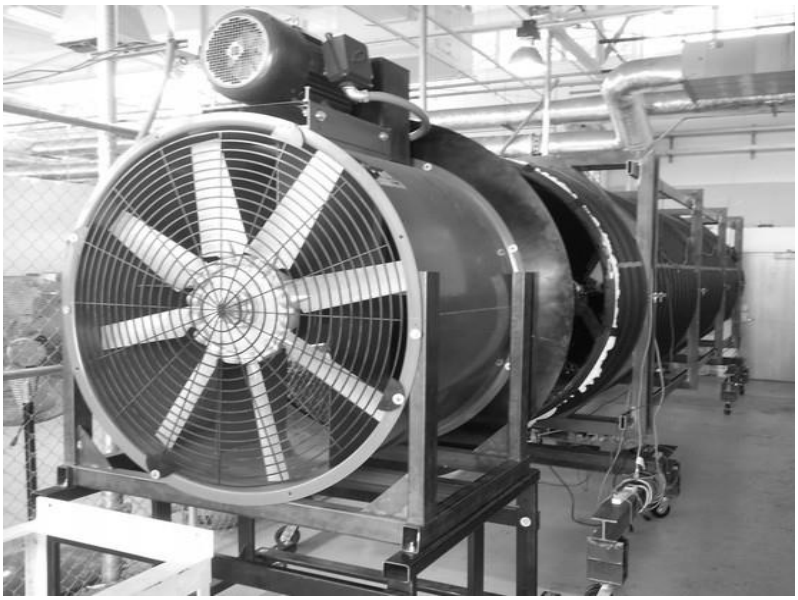

Figure 8: LDWT at SDSU's Energy Laboratory (D. W. MacPhee & A. Beyene) [5]

Following step-wise testing and data collection procedures for the experimental analysis, the rigid and morphing blade prototypes were evaluated. As per this paper's findings, the morphing blade performs up to 32.6% maximum efficiency and up to 34.5% maximum operational range over the conventional rigid blades, this shows the morphing design has better performance than the rigid blade design in all loading conditions. The numerical simulations of both rigid and flexible wind turbine blades were investigated using the k-ω-SST turbulence model through Open-FOAM [5], then the simulation and experimental results of the rotor performance for both design scenarios were compared and the experimental results were validated. Generally, the authors of this paper suggest that the morphing blade design could produce more power than a conventional rigid blade. Especially on variable load conditions. Finally, Future work was suggested in this paper to investigate "the effect of material properties and un-deformed shape on morphing behavior over a wider range of tip-speed ratios and Reynolds numbers".

J. Jauregui, et al. [40] also introduced a new morphing design concept using a flexible strip (leaf spring) on the blade along the chord of the baseline profile that is attached to the airfoil skin with rigid connecting rods, Herein the Author uses a cam mechanism to control the movement on the center of the strip. [18] Introduced another new morphing mechanism using small memory shape actuators to enable the morphing ability of the Clark-Y airfoil blade wind turbine. Generally, researchers have approved wind turbine blades with morphing ability can deliver high aerodynamic performance while replacing the conventional stiffness-driven rigid blade designs using different morphing techniques and mechanisms.

2.4. Other techniques

In addition to pitch and morphing blade control systems, numerous researchers have extensively discussed different wind turbine power control techniques such as MPPT control systems, passive and active stall control systems, and Yaw control systems. Figure 9 describes pitch and stall WT control systems. MPPT control technique is used to maximize the available wind energy based on the available wind speed, hence this algorithm helps to stabilize the power efficiency while the wind speed exceeds the cut-out speed by protecting the WT from high-stress wind load. MPPT algorithms can be further classified into two major categories. Namely, direct power control (DPC) which maximizes output electrical power, and indirect power control (IPC) algorisms which maximizes the mechanical wind power [8]. The stall WT control system can be passive or active, However, a Passive stalled control system wind turbine has slightly twisted rotor blades, and the blades are usually bolted at the hub with a fixed twist angle, this helps to prevent the lifting force of the rotor blade and is aerodynamically capable to ensure high wind load stress during the critical wind speed values. Even though passive stall is Robust, cheaper with low complexity, and faster response for the wind loads compared to other control systems, it is low efficiency at low wind speed which causes power fluctuation at the maximum steady state due to variation of grid frequencies. Many researchers did not recommend a Passive stall control system for large-scale wind turbine applications [23].

Active stall control system has power control actuators and pitch-able blades similar to a pitch-controlled WT system, which is popular for large-scale wind turbines rated greater than 1 MW [23]. During low wind speed, rotor blades become pitched to increase the angle of attack to get a large torque rather than decreasing the angle to reduce the lift force. The active control system is more efficient than the passive stall during low wind speed conditions, while the active stall can avoid overshooting the rated power at the incoming low wind speed values. Generally, active stall WT control systems have higher power production when compared with passive stall control systems. As shown in Fig. 9. The passive stall control has a slightly higher power output during the partial load region before decreasing the power output after the

rated speed until reaches the cut-out speed, but the active control system increases the power output better than the passive control unit at the cut-out speed. The pitch control systems optimize with better efficient power control which assists with startup and emergency stop for a better control mechanism.

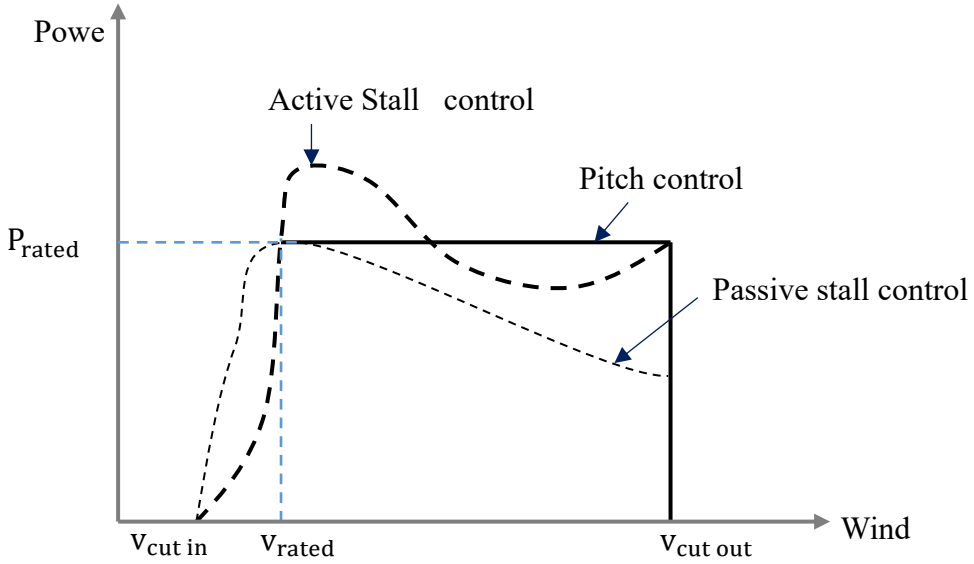

Figure 9: Pitch and stall wind turbine power control graph [8]

The Yaw control system contains a motor and drives with the main purpose of rotating the nacelle and rotor blades according to the wind direction which enables the wind turbine to capture the maximum available wind energy [23].

2.2. Proposed Morphing Blade Design

In this research project Design, 3-D modeling, and Performance Analysis of a HAWT with a passively induced morphing blade will be investigated in detail. To solve the above efficiency and lifetime problems of a conventional wind turbine, a twist-augmented bending system morphing blade inspired by a palm tree is introduced as a novel design concept. Furthermore, to address the economic advantage of morphing technologies in operational HAWT projects using life cycle comparative analysis, this paper focuses on the performance improvement of HAWT blades. This paper introduces a passively induced nature-inspired novel design approach from a palm tree with a twist-augmented bending system to improve the power efficiency and lifetime of the HAWT blades.

The detailed schematics of the concept design are shown in Fig. 10 &13. For the bending mechanism, a passively induced pivoted hinge system is introduced, with three pre-alignment blade positions which are cut in alignment, rated alignment, and stowed alignment as shown in Fig.13. The bending angle (θ) is automatically adjusted in reaction to wind speed, and to restore the bending angle to its position during low wind speed spring system is augmented with the proposed hinge system. The schematics of the novel concept morphing blade design, is shown in Fig. 10.

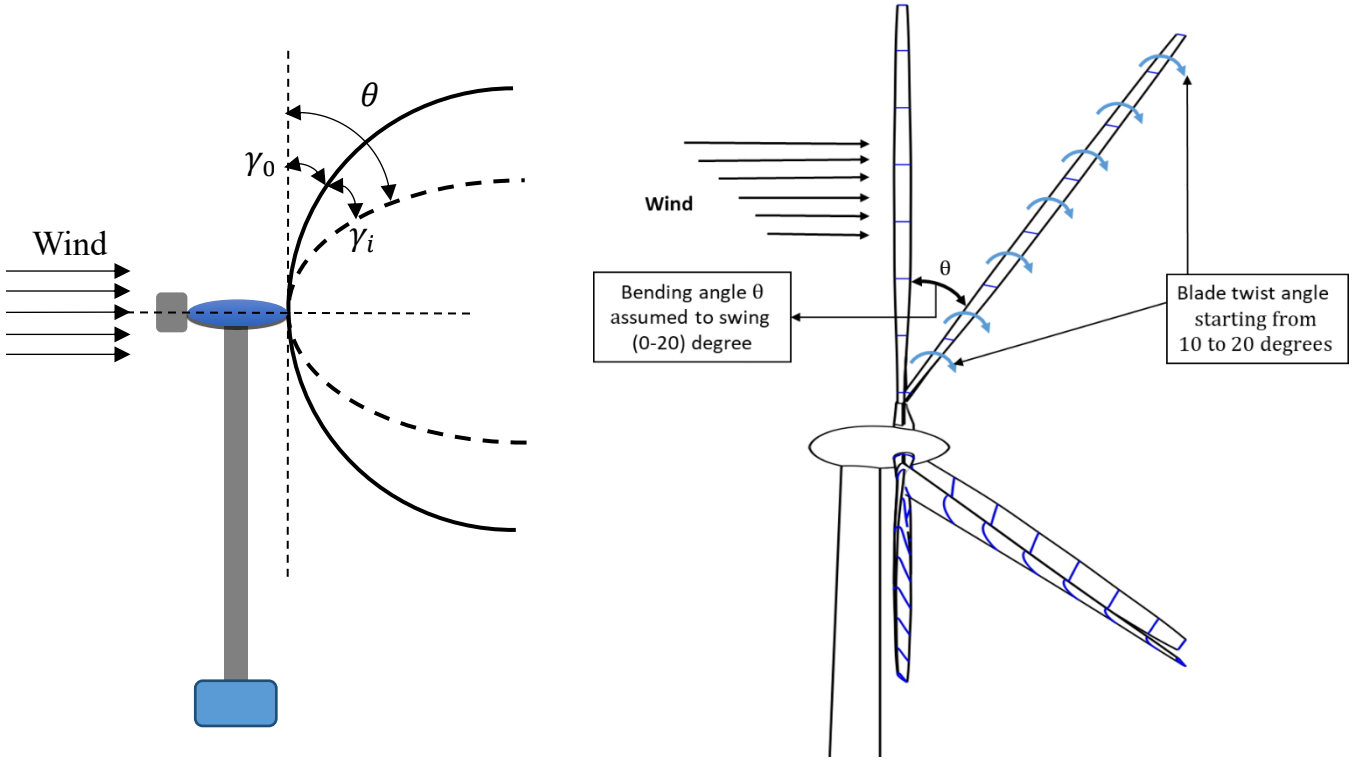

Figure 10: Schematic of palm tree-inspired morphing blade with passive control

The concept design has basic characteristics, which makes the new design approach to improve the power efficiency of the HAWTs. The wind turbine orientation is a downwind configuration to allow the rotor blades to be more flexible and able to discharge the stress on the tower at high wind speed which reduces the overall manufacturing cost of the turbine. The bending angle is automatically adjusted and the rotor blade can fold and unfold upon itself passively by exploiting a pivot hinge in the reaction of wind speed. To restore the blade bending angle to its position during low tip speed ratio a spring system is augmented with the proposed hinge system design. The proposed material for the blade is assumed to be carbon fiber, it is known that glass fiber is a common blade material but carbon fiber is lighter, which dictates a maximum bending angle. The design should allow a higher tip speed ratio. Depending on the wind speed the blade is assumed to swing from (0-20) degrees. As shown in Fig. 10, the bending angle (θ) is the summation of the pre-aligned ranges which is $\theta = \gamma_0 + \gamma_i$.

Chapter Three: Methodology

3.1. Progressive steps of the research

To address systematically the intended objectives of this research project, a detailed methodology was followed. Conducting a literature review on wind turbine profiles, design techniques, and performance ranges was the first step, then the wind turbine blade part load issue was followed. After that, the NACA Applicable profiles for the morphing blade design have been selected, and all types of modeling for the selected blade profile were investigated in detail. The design compatibility analysis (DCA) of the proposed design is also part of the project work. Software packages such as CERO PTC 8 for 3D modeling and ANSYS Fluent 2021R2 for CFD modeling are used. Finally, to estimate how much efficiency is increased, the life cycle comparative analysis of the morphing blade, with reference site of the Adama II wind farm project annual energy conversion capacity will be studied. Generally, the progressive steps of research work are summarized using a flowchart as follows.

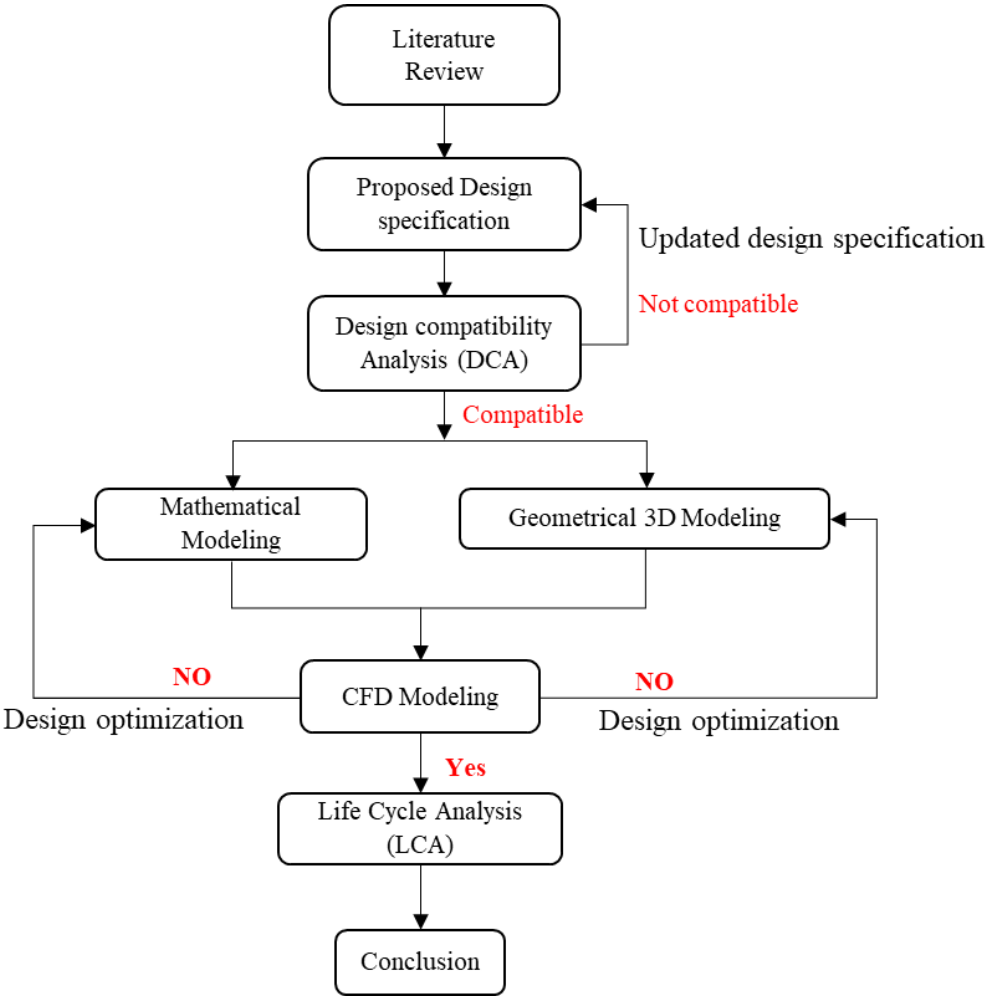

Figure 11: Methodology and progressive steps of research work

3.2. Analytical Modeling

3.2.1. Design Specification of the proposed morphing blade

Herein a passively induced bio-inspired new design approach from a palm tree is introduced as a concept design. In this novel design approach, the rotor speed is regulated by a twist-augmented bending system and the blade restoration at low wind speed is performed by a spring-augmented pivot hinge system.

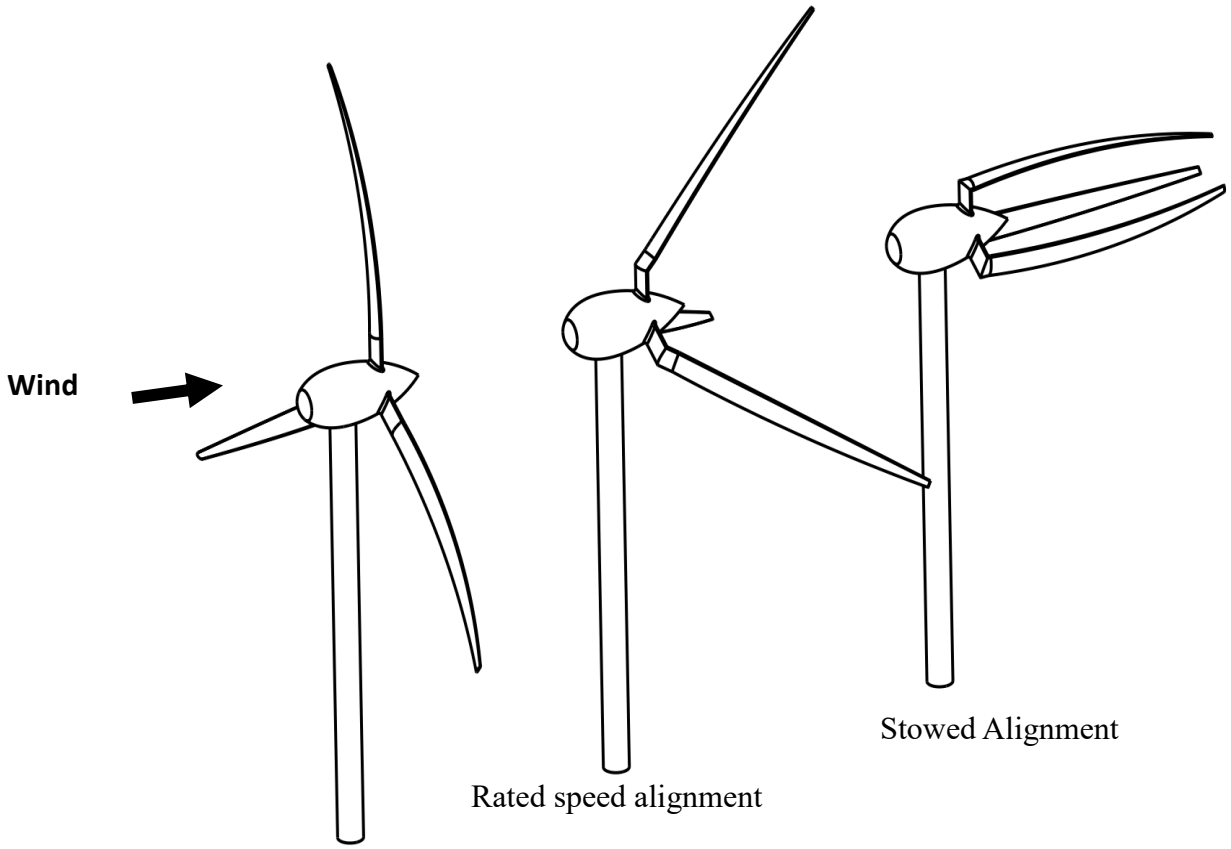

Figure 12: Palm tree inspirited morphing blade HAWT pre-aligned blade positions

The general specification and assumptions of the proposed morphing blade design are as follows.

- The concept design of the morphing blade is inspired by a palm tree.
- The HAWT is three-bladed with a twist-augmented bending system.
- The wind turbine orientation is with a downwind configuration
- The blades will fold and unfold upon themselves by exploiting a pivot hinge in reaction to wind speed.

- To restore the bending angle to its position during low TSR a spring system is augmented with the proposed hinge system design.
- The material for the blade is assumed to be carbon fiber.
- The design should allow a higher Tip speed ratio, and depending on the wind speed the blade is assumed to swing from 0-20 degrees.

The partial design, specification is assumed to calculate the remaining design parameters. The rated wind speed is site-specific, for comparison purposes in the next chapter of the life cycle analysis, the site-specific wind speed parameters were taken from the Adama II wind farm project.

Table 1: Partial assumption of proposed design specifications from SANY SE7715 wind turbine.

Parameters	Values
Number of Blades	3
Rotor diameter	77 m
Cut-in speed	3 m/s
Rated wind speed	11.5 m/s
Hub height	70 m

The assumptions of the design parameters will be cross-checked if it is rightly assumed by calculating the Power as a function of TSR, efficiency, radius, and wind speed analytically. Based on translational momentum theory [24], the theoretical amount of energy and power generated from a specific wind turbine technology can be calculated analytically. Here is the theoretical power extracted from an available wind speed (v) passing through a swept area A can be expressed mathematically as,

$$P_w = \frac{1}{2}\rho A v^3 \ldots\ldots\ldots\ldots\ldots\ldots\ldots\ldots \quad (3.1)$$

Where A is the swept area of the rotor blade, for the fixed pitch rigid blade conventional horizontal axis wind turbine the swept area can be calculated using the following equation:

$$A = \prod R^2 \ldots\ldots\ldots\ldots\ldots\ldots\ldots\ldots \quad (3.2)$$

In this proposed morphing blade design unlike the conventional wind turbine, the swept area is not constant, it depends on the bending angle of the rotor blade. To increase the power efficiency and lifetime of the HAWT wind turbine, the swept area reduces as the maximum wind speed becomes worst and the bending angle increase. Hence there will be a different swept area in Cut-in, Rated, and cut-out alignments depending on the availability of wind energy.

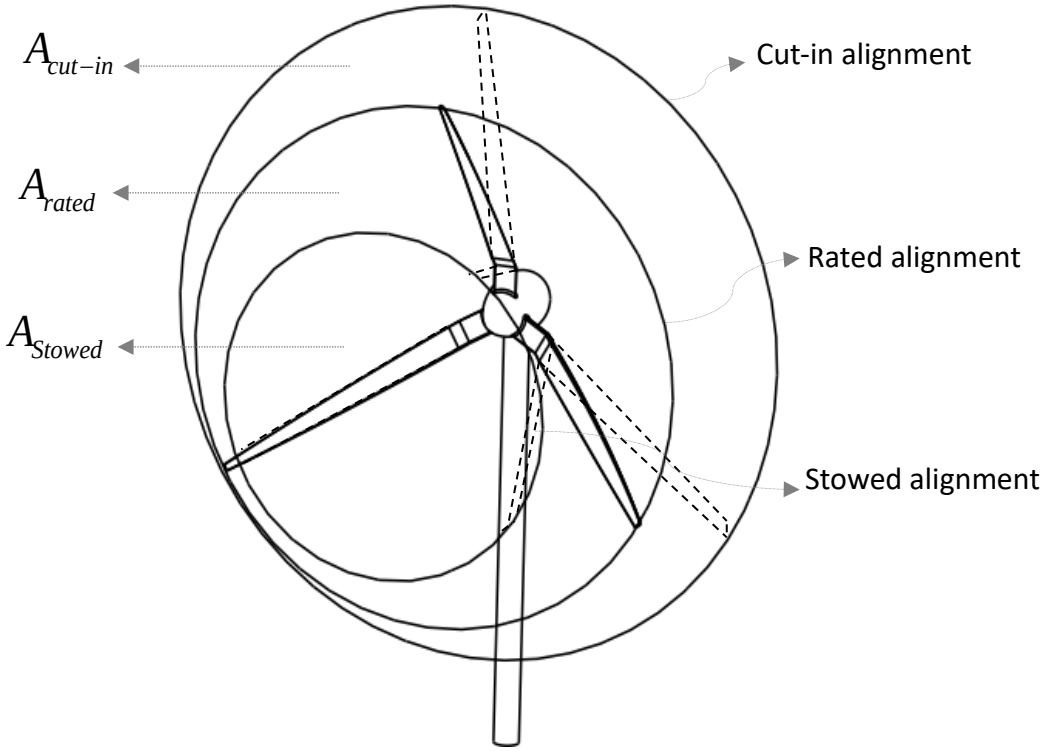

Figure 13: Palm tree inspirited morphing blade swept area at different alignment

Figure 13, illustrates the range of the swept area at different rotor blade alignments. Here the rotor blades will fold and unfold passively upon themselves by exploiting a pivot hinge in the reaction of wind speed, in principle, it is seen at 90 degrees bending angle, and the power output will be about zero. Therefore, the proposed design considers the rotor blade swings with a bending angle of 0°-20° to produce the maximum power output by keeping the higher tip speed ratio within the specified range of swept area.

Mathematically we can model the above representation in two-dimensional analysis to calculate the swept area at different bending angles as shown below.

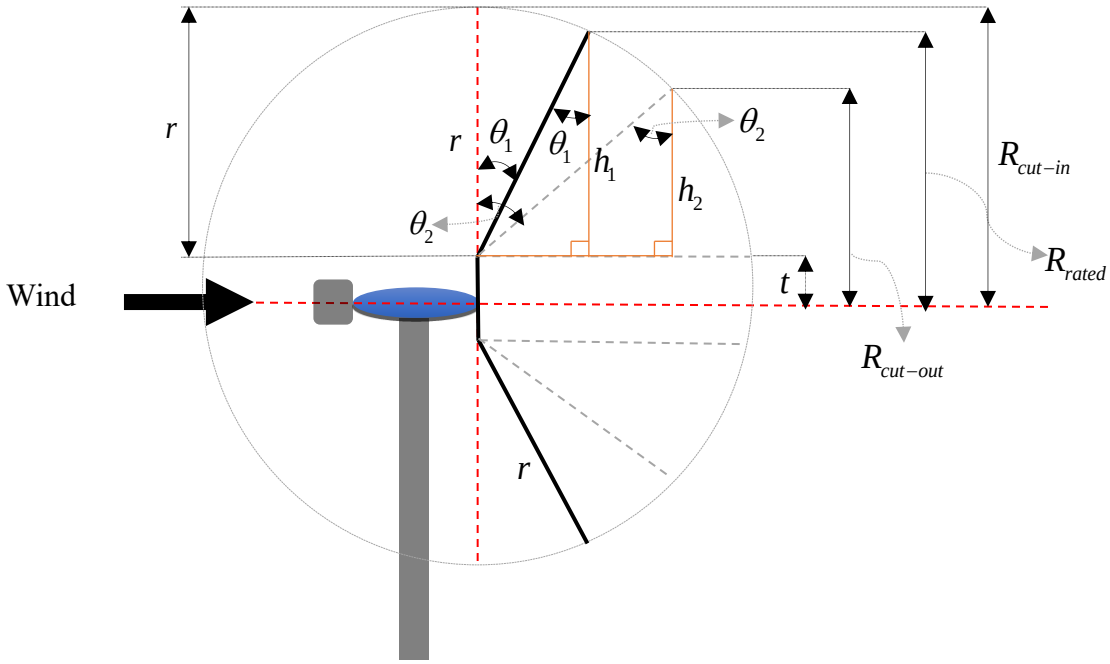

Figure 14: 2D representation of morphing blade swept area alignments

From the above schematics, we can calculate the radius of the swept area at different bending angles using the trigonometric principle as shown below.

$$\left.\begin{aligned} &R_{cut\_in} = t + r \\ &R_{Rated} = t + h_1 \gg t + r\cos\theta_1 \\ &R_{cut\_out} = t + h_2 \gg t + r\cos\theta_2 \\ &\vdots \\ &R = t + h \gg t + r\cos\theta \end{aligned}\right\} \ldots\ldots\ldots\ldots\ldots\ldots\ldots\ldots \quad (3.3)$$

Therefore, by substituting equation 3.3 in equation 3.2, the swept area at any bending angle (θ) of the proposed morphing blade design can be calculated as follows.

$$A = \prod(t + r\cos\theta)^2 \ldots\ldots\ldots\ldots\ldots\ldots\ldots\ldots\ldots\ldots \quad (3.4)$$

Where t is the root length from the center of rotation to the bending hinge, and h is the height adjacent to the bending angle θ which is the product of the rotor radius and the cosine of the bending angle. From the above assumption of the rotor radius of 38.5 meters, we can assume the root length (t) which is the length from the rotor axis to the bending point as 8 meters Fig. 15, and the cord length of the blade (r), which is the length from the bending point to the tip blade as 30.5 meters to calculate the swept area at any bending angle using equation 3.4.

Therefore, using the equations 3.1 and 3.4, the power extracted from proposed morphing blade ant any bending angle θ can be calculated mathematically as follows.

$$P_T = \frac{1}{2}\rho\prod\left(t + r\cos\theta\right)^2 v^3 \ldots\ldots\ldots\ldots\ldots\ldots \text{(3.5)}$$

And the torque of the fixed-pitch blade wind turbine can be calculated explicitly as follows.

$$\tau_T = \frac{P_T}{\omega} \gg \frac{1}{2}\rho\prod\left(t + r\cos\theta\right)^2 \left(\frac{v^3}{\omega}\right) \ldots\ldots\ldots\ldots \textit{(3.6)}$$

Another critical design parameter in wind turbine design is the power coefficient (Cp), which is a measure of the combined efficiency of the wind turbine system components. Power coefficient (Cp) can be expressed as the ratio of produced power by a wind turbine divided by the total wind power flowing into the turbine blades at a specific wind speed [25].

$$Power\ coefficient(Cp) = \frac{Turbine\ power}{power\ of\ wind} \ldots\ldots\ldots\ldots\ldots\ldots\ldots \text{(3.7)}$$

In this paper for the proposed morphing blade design, the power coefficient (Cp) is a function of tip speed ratio (TSR), twisting, and bending angles. Whatever the energy conversion device the theoretical maximum power coefficient (Cp) from available wind power is about 59.3% [40]. However, real wind turbine generators do not reach this theoretical maximum power coefficient (Cp). Research indicates that the practical power coefficient (Cp) is between 0.4 and 0.5 for fixed-pitch industrial wind turbines [2].

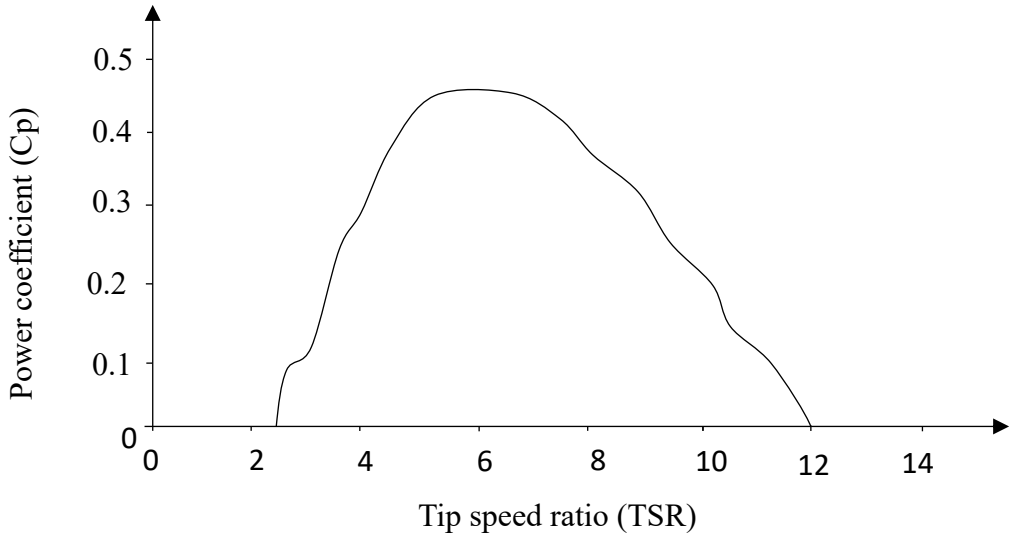

Figure 15: Power coefficient (Cp) Vs Tip speed ratio (TSR) for fixed pitch angle

Tip Speed ratio (TSR) is one of the critical design parameters in wind turbine technology, which is used to optimize the blade design to capture the maximum amount of energy from the available wind speed. TSR is the ratio of the tangential velocity of the tip rotor divided by the available wind speed.

$$TSR = \frac{Tangential\ velocity\ of\ the\ Tip\ Rotor}{Wind\ speed} \gg \frac{\omega R}{v} \quad \ldots\ldots\ldots\ldots\ldots\ldots\ldots \quad (3.8)$$

According to previous researcher investigation [26] .without going into the detailed mathematical calculation, the approximate TSR values for different blade orientations are given in Table 2.

Table 2: TSR values for different blade orientations [26]

No of blades (N)	TSR Value
2	$\sim 6-7$
3	$\sim 5-7$
5	$\sim 2-3$

Therefore, considering the three-bladed proposed morphing blade design should allow a higher tip speed ratio while the blade swings from 0-20 degrees based on the availability of wind speed the better assumption for the TSR value is 7.

In modern wind turbine technology twist angle is added along the blade length to optimize the energy harvested from the available wind speed. Hence for most wind turbine blade designs 10° to 20° of twist angle is added with a maximum twist angle at the tip of the blade [27] Therefore, it is possible to assume the twist angle from 10° to 20° for the proposed design. The advantage of adding a twist angle in the proposed morphing blade design is to change the apparent wind direction across the blade. In general, the theoretical calculation was performed using different bending angles, starting from 0° to 20° based on Blade element momentum theory (BEMT). The calculated design parameters at different bending angles are summarized as follows (table 3&4).

Table 3: The summary formula for the design parameters

Description	Formula	Remark
Swept area (A)	$A = \prod(t + r\cos\theta)^2$	Root length (t) is assumed to be 8 m.
TSR	$TSR = \frac{Tangential\ velocity\ of\ the\ Tip\ Rotor}{Wind\ speed} \gg \frac{\omega R}{v}$	The assumed Max TSR value is 7.0
Power coefficient (C_p)	$Power\ coefficient(C_p) = \frac{Rated\ Turbine\ power}{power\ of\ wind}$	Rated power is calculated at V_{rated} = 11.5 m/s
Power	$P_T = \frac{1}{2}\rho\prod\left(t + r\cos\theta\right)^2 v^3$	The density of air is 1.225 kg/m3
Torque	$\tau_T = \frac{P_T}{\omega} \gg \frac{1}{2}\rho\prod\left(t + r\cos\theta\right)^2\left(\frac{v^3}{\omega}\right)$	The diameter depending on the bending angle
Angular speed (ω)	$\omega = 2\left(\frac{TSR\ x\ Rated\ speed}{Diameter}\right)$	V_{rated} = 11.5 m/s
Tip speed (V_{Tip})	$V_{Tip} = V_{rated}\ x\ TSR$	Root length (t) is assumed to be 8 m.

Table 4: Summary of theoretical (analytical) results

Bending angle	Diameter (m) $D = 2(t + r\cos\theta)$	V_{rated} (m/s)	TSR	V_{Tip} (m/s)	ω (rad/s)	Swept area (m2)	Power (W)	C_p
0°	77.000	11.50	7.0	78.75	2.045	4654.265	$4.06\,x10^6$	0.42
10°	75.927				2.074	4525.505	$3.95\,x10^6$	0.43
15°	74.594				2.111	4367.990	$3.81x10^6$	0.45
20°	72.742				2.165	4153.782	$3.62\,x10^6$	0.47

3.2.2. NACA selection and structural reliability

3.2.2.1. Applicable profiles and selection

Wind turbine rotor blades are the most fundamental component of wind turbine technology, which uses airfoils to produce mechanical power [28]. In airfoil terminology, the geometric parameters that affect the

aerodynamic performance of an airfoil include the leading edge, camber line, cord line, and trailing edge angle [4].

Figure 16 shows the detailed geometric parameters of a two-dimensional typical airfoil structure.

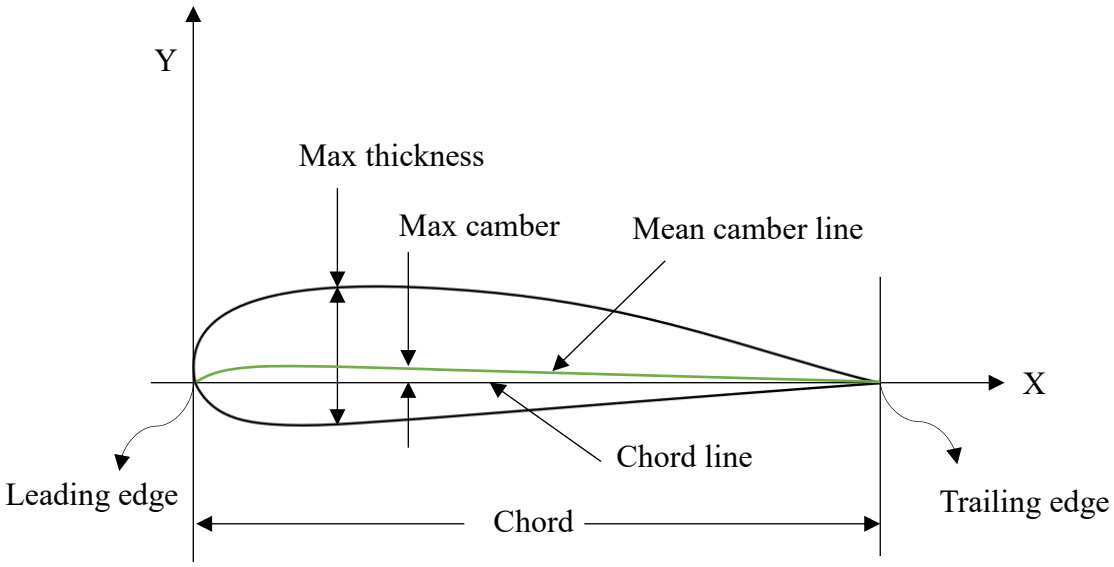

Figure 16: Airfoil nomenclature

To optimize the cost of energy and life cycle issues, aerodynamics and structural reliabilities are the most critical design consideration in wind turbine blade design. The aerodynamic factors that affect the blade designs are Airfoil, design-rated power, wind speed, tip speed ratio (TSR), Solidity, Number of blades, and rotor orientation, and depending on their application, there are many types of airfoils [29], and some of the most common generic shapes of airfoils are, under-cambered, Flat-Bottom, Semi-Symmetrical, symmetrical, reflexed, Kline–Fogelman and Flat Airfoils.

In this paper, NACA 4412 airfoil is selected for the proposed morphing blade with a max thickness of 12% at 30% chord and max camber of 4% at 40% chord. Due to its nearly flat bottom surface, the overall advantage of the NACA 4412 airfoil for the proposed morphing blade is, it prevents the negative ground effect that occurs with the extreme camber while the venturi flow is created below the airfoil [30], From the UIUC airfoil coordinates database the top and bottom coordinates of the NACA 4412 selected airfoil are imported to model the profile using Cero PTC 8 as shown below.

3.2.2.2. Material Selection and structural reliability

The objective of selecting suitable blade material for this proposed morphing blade is to assess commercially available and cost-effective material, specifically suitable to resist the intermittent loading nature of the wind turbine blades. Researchers indicated that the most common materials for wind turbine rotor blade constructions are, fiberglass and carbon fiber.

In this paper, carbon fiber is selected as a suitable material for the proposed morphing blade design. because carbon fiber is the most researchers suggested rotor blade material due to its significant advantage over fiberglass with improved stiffness, strength, and fatigue resistance per unit mass, hence these properties of the carbon fiber material reduce the mass of wind turbine blades to increase the overall aerodynamic performance and a lifetime of the wind turbine blades [31]. The technical data of the selected carbon fiber material (Zoltek Px35 Carbon Fiber) is found in the Zoltek Carbon Fiber company datasheet which is the largest carbon fiber supplier to the Wind Industry [32]. The primary consideration in the blade structural design is, its structural reliability to withstand static, steady, cyclic, impulsive, stochastic, transient, and resonance loads at normal and extreme conditions. However, these important considerations focus on the material and blade fabrication options.

Historically, wind turbine blades were made from wood and steel. Since the 1970s, most blades of HAWT blades have been made from composites such as fiberglass [33] Nowadays carbon fiber is the most common blade material due to its lightweight and economically cost-effective material with improved stiffness and better fatigue lifetime. In this proposed morphing blade design carbon fiber is selected as blade material and the aspiring system is augmented to restore the bending angle to its position during low TSR, however, this makes the blade structure more reliable. The design reliability depends on the material selection, therefore the primary consideration in the blade structural design is, its structural reliability to withstand loads conditions at normal and extreme wind loads. In this case the expected loading conations are figured out using force components as shown Fig.18. Therefore the material is expected to withstand those force components exerted on the rotor assembly at the intermittent wind loads.

Figure 18, is the side view of downwind rotor assembly force components at a particular span-wise location.

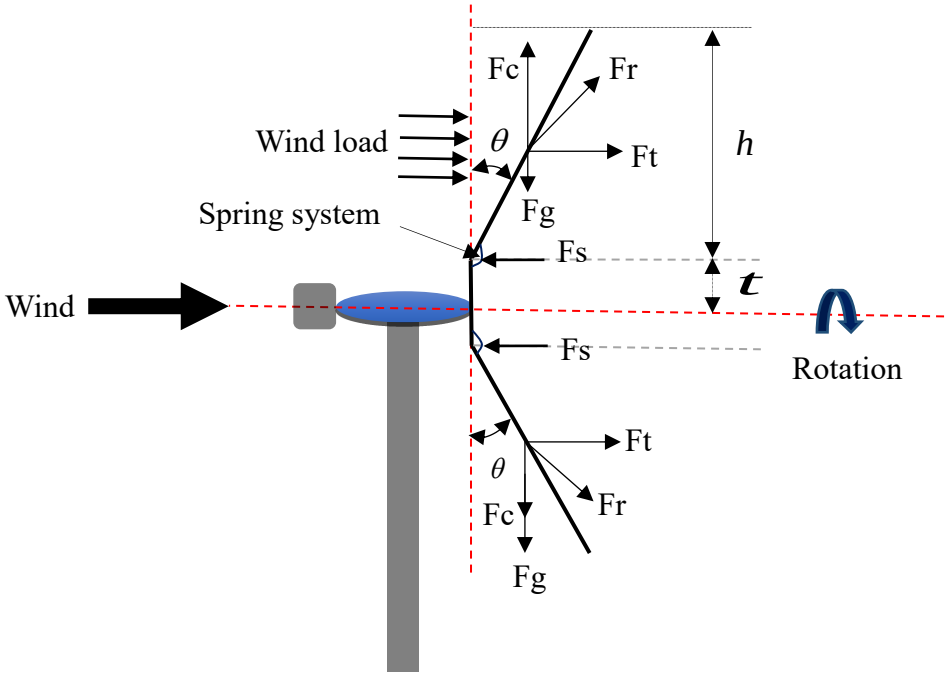

Figure 17: Side view of downwind rotor assembly force components

Figure 17, shows the schematic of force components for an extreme-scale three-bladed wind turbine with a downwind configuration with a particular span-wise location. As shown in the picture there are four force components namely, Centrifugal force (Fc), Trust force (Ft), gravitational force (Fg), and spring force (Fs) to restore the blade position at low TSR values. The centrifugal force (Fc) acts in the radial direction of the rotor blade and it is a function of angular velocity (ω), the mass of the blade (m), and radial distance (r).

$$F_C = \omega m r^2 \quad \text{..... (3.10)}$$

The gravitational force (Fg) also acts in the radial span-wise direction of the rotor and it is a function of the mass of the blade (m) and acceleration due to gravity (g).

$$F_g = mg \quad \text{..... (3.11)}$$

It is not as simple as to model the thrust force (Ft), like the centrifugal and gravitational force, because it involves more complex distribution due to its highly-coupled three-dimensional aerodynamic flow behavior. Researchers developed a baseline differential thrust distribution for the conventional blade configuration with bending angle (θ) as follows [34].

$$F'_T = F'_{T,c}\cos^2(\theta) \quad \ldots\ldots\ldots\ldots\ldots\ldots \quad (3.12)$$

The spring force (Fs) in the proposed morphing blade design helps to restore the blade position at low TSR values. Like the trust force, the spring force has also complex distribution and needs more investigation which is left as a future work in this paper. Simply we can express the spring force as a function of the spring constant (k) and the distance x.

$$F_s = kx \quad \ldots\ldots\ldots\ldots\ldots\ldots\ldots\ldots \quad (3.13)$$

Therefore, the resultant force (Fr) for an extreme-scale three-bladed wind turbine with a downwind configuration for a particular span-wise location can be calculated as follows.

$$F_r = F_c + F_g + \left(F_t - F_s\right) \quad \ldots\ldots\ldots\ldots\ldots \quad (3.14)$$

Generally, the structural consistency of the proposed morphing blade to withstand various loads at normal and extreme conditions depends on material selection and loading conditions. However, Zoltek Px35 Carbon Fiber is selected as a blade material and the spring system is augmented to restore the blade position while morphing at low TSR values.

Table 5: Summary of the design parameters

Parameters	Values
Number of Blades	3
Rotor diameter	77 m
Cut-in speed	3 m/s
Rated wind speed	11.5 m/s
Hub height	70 m
Blade Arifol	NACA 4412
Blade material	Zoltek Px35 carbon fiber
Average Rated power	1.8 MW
Twist angle	10° to 20°

3.3. Design compatibility of the proposed morphing blade

3.3.1. Framework of the compatibility analysis (DCA)

K. Ishii et al. [6], develop a general framework for design compatibility analysis of knowledge-based computer tools that encourage simultaneous engineering in mechanical design. In this paper, design compatibility analysis (DCA) aims to study the compatibility between the required design requirements and the proposed morphing blade design. However, based on compatibility knowledge, concerning the critical points on functionality, manufacturability, morphing ability, reliability, and other life cycle design issues, the proposed HAWT morphing blade will be evaluated, justified, and suggested for further improvements in the early design stage. The authors used a fundamental strategy of DCA Fig. 12, to study the compatibility analysis of coal-fired power plants. Hence, the same DCA strategy will be followed to study the compatibility analysis of the proposed morphing blade.

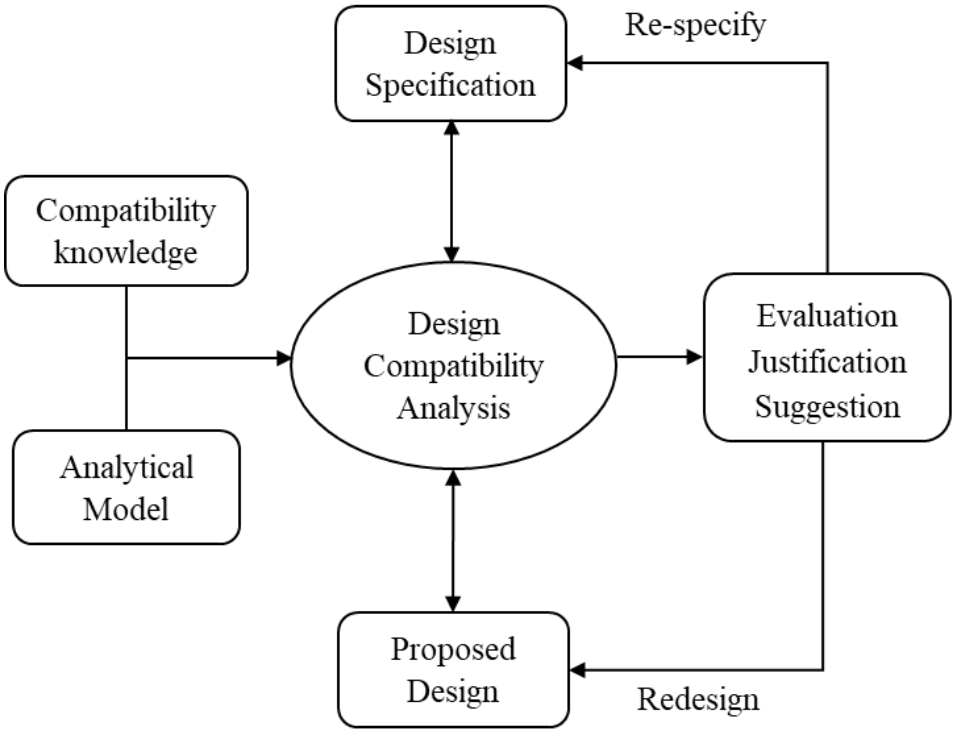

Figure 18: Flow chart concept of compatibility design analysis (DCA) [6]

Figure 12, the technical design specification for the proposed design will be described first. The design specification of the proposed design can be some part of the entire system, the remaining design specification will be decided based on some assumptions and analytical calculations. Once all design requirements are fulfilled, using the compatibility knowledge the proposed design specification will be evaluated and justified to put suggestions for further improvement.

3.3.2. DCA implementation for the proposed morphing blade

A knowledge based mathematical decision analysis, based on the expert's subjective evaluation scale for the compatibility degree of confidence named as utility theory is developed K. Ishii et al. [1] was used for the DCA implementation of the proposed design. This theory uses a normalized scale called match index (MI) to justify the evaluation of the proposed design and suggestions for further improvements. The mathematical decision analysis of utility theory as per K. Ishii et al. [1], investigation uses to calculate the match index (MI) as follows. Consider the proposed morphing blade design has a set of design considerations K.

$$MI = \sum_k utility(p).M(p) \quad S \in K \ldots\ldots\ldots\ldots\ldots\ldots\ldots\ldots\ldots\ldots\ldots\ldots (3.15)$$

Where, utility (p) is the weight of evaluation for the comparability parameter p, ∑utility (p) = 100%, and M (p) is the compatibility of parameter p, (∑M (p) = 1.0). Table 6 indicates the degree of confidence for the proposed design based on match index (MI) values.

Table 6: Degree of confidence vs Match index (MI) values [6]

Match index (MI)	Degree of confidence
0	Absolute incompatible design
0.5	No compatibility information is available
<0.5	Incompatible design
>0.5	Compatible design
1	Perfectly compatible design

For an acceptable design, the Match index (MI) value for the proposed morphing blade design has to be greater than 0.5. Herein the compatibility parameters for the proposed morphing blade design are manufacturability, functionality, reliability, serviceability, lifetime, cost, morphing ability, assembly, efficiency, and blade weight. However, based on the compatibility knowledge and prior researchers' investigations on morphing blade design the compatibility of the above parameters for the proposed morphing blade is given in the table below.

Table 7: Compatibility analysis of the proposed morphing blade design

Compatibility Parameters utility (p)	Weight of evaluation Utility (p)	Compatibility of parameter p M(p)
Manufacturability	10%	0.8
Functionality	14%	0.9
Reliability	12%	0.85
Serviceability	9%	0.6
Lifetime	11%	0.75
Cost	13%	0.85
Morphing ability	9%	0.95
Assembly	8%	0.8
Efficiency	9%	0.85
Blade weight	5%	0.95
$Match\ index(MI) = \sum_k utility(p).M(p)$		0.83

It is also possible to represent the DCA evaluations for different design parameters in a so-called amoeba chart [6], as shown in Fig. 19. The amoeba chart is commonly used to help experts make multiple objective decisions using a unity circle, lines inside the circle are the DCA score lines for each design parameter.

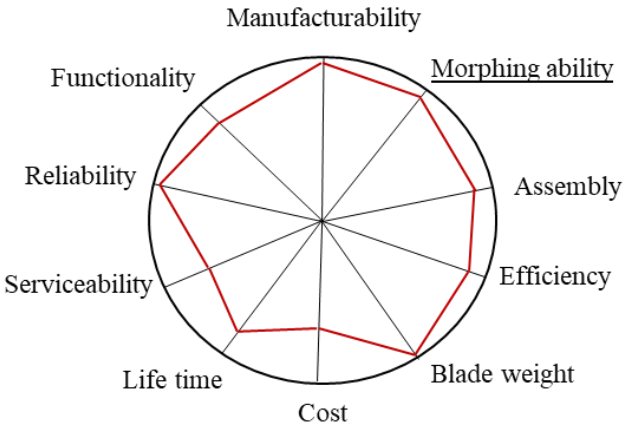

Figure 19: Amoeba chart for DCA scores

Generally, from the above DCA analysis the match index (MI) is 0.83 which is greater than 0.5, therefore based on knowledge-based compatibility analysis the proposed morphing blade is compatible.

3.4. Modeling and analysis

3.4.1. Modeling tools and approaches

After investigating the detailed design compatibility analysis (DCA) of the proposed morphing blade design, the novel design approach is confirmed as a compatible design based on the researcher's compatibility knowledge within the given design specifications. Hence to address the intended objectives of this research project 3D numerical analysis using a software package is followed in this section. However, CERO PTC 8 software package is used for 3D modeling and ANSYS Fluent 2021R2 is used for aerodynamics analysis of the rotor blade at different bending angles using the CFD turbulence model. Herein the detailed approach of the 3D modeling and CFD analysis will be investigated in detail. The 3D modeling of the proposed novel morphing rotor blade design is a twist-augmented bending system inspired by the palm tree. The blade design is based on the NACA4412 profile and it is with a 3-meter cord length and 38-centimeter maximum thickness at the root and a 1.03-meter cord length and 13-centimeter maximum thickness at the tip of the rotor blade. In addition to the above specifications, the rotor blade model has a twist angle starting from 10 to 20 degrees which increases to the tip of the rotor blade. The picture below shows the 3D model of the typical proposed wind turbine design at different bending angles.

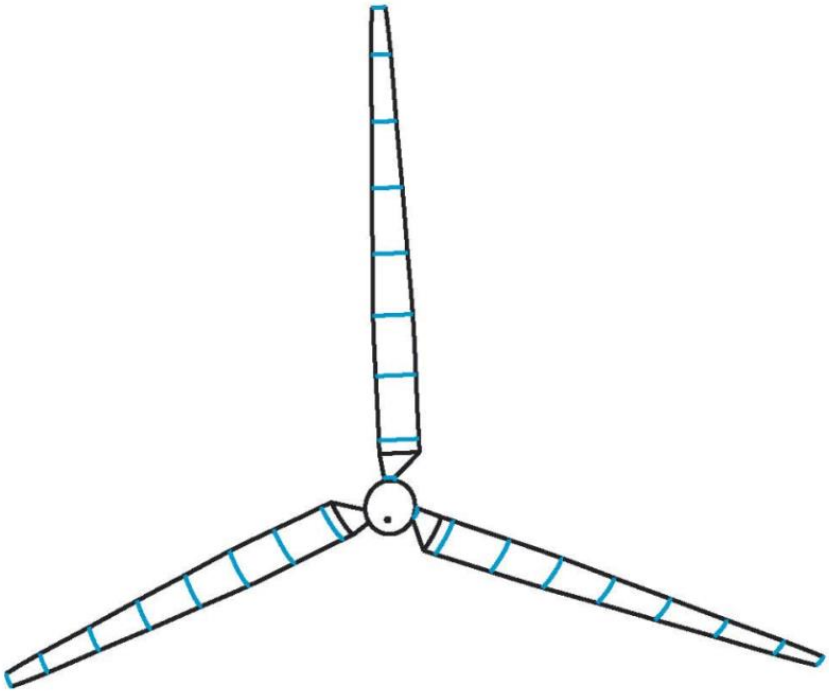

Figure 20: 3D modeling of the morphing blade assembled with hub

Generally, the geometry of the proposed palm tree-inspired horizontal axis wind turbine rotor blade will have different swept areas at different bending angles as specified in above Table 4.

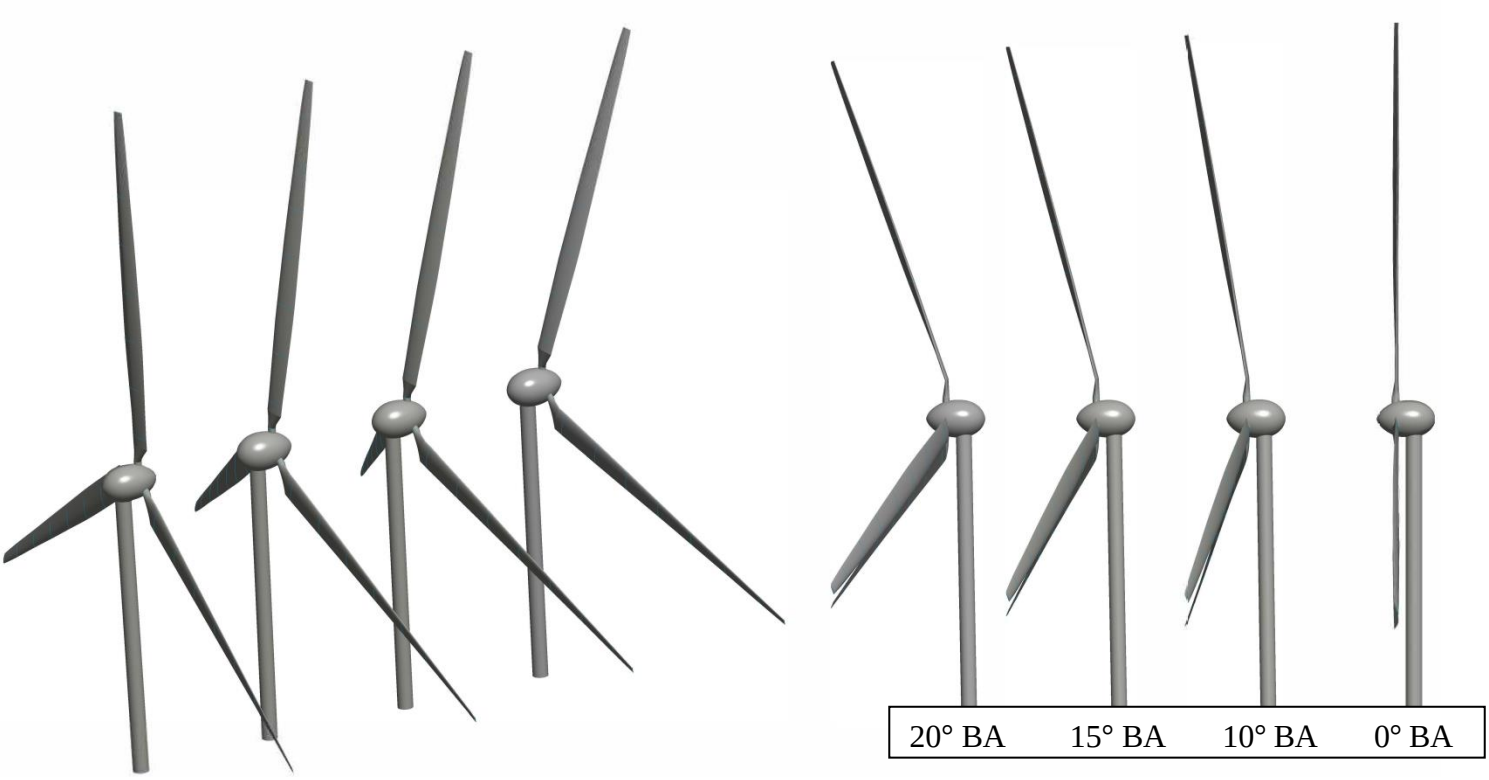

Figure 21: 3D modeling of the morphing blade at different bending angles

Figure 18 shows the 3D model of the novel design approach with four models at different bending angles, the four parametric models have [77, 75.927, 74.594, and 72.742] meter rotor diameters with 0°, 10°, 15°, and 20° bending angles respectively. The diameter of the rotor area is calculated analytically from the above principle as shown in Fig. 14.

$$D = 2(t + r\cos\theta) \ldots\ldots\ldots\ldots\ldots\ldots\ldots \quad (3.16)$$

Where "t" is the root length from the center of the hub assumed to be 8 meters, and "r" is the radius after bending from the pivoted hinge system as shown in Fig. 14. Hence the swept area of the rotor blade is different with different bending angles this helps to withstand the extreme wind loads with better morphing ability by reducing the swept area of the rotor blade passively to maximize the power efficiency and increase the lifetime of the turbine.

3.4.2. Computational Analysis

The computational analysis of the proposed morphing blade design is based on simplified Reynolds Averaged Navier-Stokes (RANS) governing equation called Spalart-Allmaras (SA) turbulence model. This model is single equation turbulence model to describe transport equation for eddy viscosity, which is primarily developed for the aerodynamic applications [26]. The advantage of using SA turbulence model is, its compatibility for boundary layer flows with variable pressure gradients and capability of complexity problem reduction to save the computational time. The SA turbulent model fundamental governing equations is defined as:

$$\frac{DF}{Dt} = \frac{\partial F}{\partial t} + (u.\nabla)F \quad \text{..... (3.17)}$$

Expanding the equation for full model for transport equation of the working variable $\hat{v}$ is defined as:

$$\frac{\partial \hat{v}}{\partial t} + \hat{u}_j \frac{\partial \hat{v}}{\partial xj} = C_{b1}\hat{S}\hat{v} + \frac{1}{\sigma}\left[\frac{\partial}{\partial xj}\left((v+\hat{v})\frac{\partial \hat{v}}{\partial xj}\right) + C_{b2}\frac{\partial \hat{v}}{\partial xj}\frac{\partial \hat{v}}{\partial xj}\right] - C_{w1}f_w\left(\frac{\hat{v}}{d}\right)^2 \quad \text{.....(3.17)}$$

The eddy viscosity (μ_t), damping function (f_{vn}), magnitude of the vorticity ($\hat{S}$) and destruction function (f_w), is also defined as:

$$\left.\begin{aligned}
&\text{Eddy Viscosity } (\mu_t) \\
&\mu_t = \bar{\rho}\hat{v}f_{v1} \\
&\text{Damping function } (f_{vn}) \\
&f_{v1} = \frac{x^3}{x^3 + (c_{v1})^3},\ f_{v2} = 1 - \frac{x}{1 + xf_{v1}},\ and\ \ f_{v3} = 1 \\
&\text{Magnitude of the vorticity } (\hat{S}) \\
&\hat{S} = f_{v3}\sqrt{2(\Omega_{ij})^2} + \frac{\hat{v}}{k^2 d^2} f_{v2} \\
&\Omega_{ij} = \frac{1}{2}\left[\frac{\partial \hat{u}_i}{\partial x_j} - \frac{\partial \hat{u}_j}{\partial x_j}\right] \\
&\text{Destruction function } (f_w) \\
&f_w(g) = g\left[\frac{1 + (c_{w3})^6}{g^6 + (c_{w3})^6}\right],\ g = r + C_{w2}r(r^5 - 1) \\
&r = \frac{\hat{v}}{\hat{S}k^2 d^2},\ and\ c_{w1} = \frac{c_{b1}}{k^2} + \frac{(1 + c_{b2})}{\sigma}
\end{aligned}\right\} \quad \text{..... (3.19)}$$

For the numerical analysis using ANSYS Fluent 2021R2, here are the assumptions applied to the above SA governing equation (3.19).

- The flow is incompressible flow, and the effect of molecular velocity is neglected
- Assume the fluctuations along the flow change to zero
- Assume the flow is stationary concerning the mean velocities

The external ambient wind field is modeled as an external fluid model and the inlet and outlet boundary conditions are assigned within the external fluid model. The proposed morphing blade HAWT is represented by its hub height, rotor diameter, bending angle, and blade twist angle. There will be two simulation scenarios proposed to perform based on the bending angle of the rotor blade while keeping the maximum tip speed ratio as a basic design consideration. The wind flow is assumed towards the negative z-direction. Considering the Novel design should allow a higher tip speed ratio while the blade swings from 0°- 20° bending angles based on the availability of wind speed the reasonable assumption for the large wind turbine TSR value is 7. Herein the blade is assumed to rotate clockwise direction along the negative z-axis with a downwind configuration. Using the assumed TSR value, rated speed, and radius of the rotor blade at different bending angles (0°,10°,15°,20°) the rotational angular velocity is calculated mathematically as (2.045,2.074,2.111,2.165) rad/s respectively.

In general, the following boundary conditions are applied to the computational model to investigate the aerodynamic characteristics of the blade geometry at different bending angles.

- The operating pressure was maintained to be 101325 Pa.
- The inlet boundary condition is 11.5 m/s rated velocity and 7.75 m/s annual average velocity with 5% turbulent intensity and turbulent viscosity ratio of 10.
- The outlet boundary condition is the gauge pressure at 1 atm.
- The blade is with no-slip boundary conditions and
- The sides are with periodic boundary conditions at 120°.

The mesh is generated in ANSYS workbench 2021R2 then boundary conditions are applied using ANSYS Fluent 2021R2. The summarized physics model and boundary conditions of the CFD analysis is shown in the table below.

Table 8: Physics model and boundary conditions on ANSYS Fluent

Physics model and boundary conditions on ANSYS Fluent		
	Solver	ANSYS2021 R2
Flow model	Time	Steady-state
	Equation of state	Constant density
	Blade diameter material	77 m
	Blade Airfoil	NACA 4412
Model proprieties	Blade material	Zoltek Px35
	Bending angle	(0°,10°,15°,20°)
	Fluid	air
Turbulence model	Viscos model	Spalart-allmaras turbulence model
boundary conditions	Inlet velocity	7.75 m/s, 11.5 m/s
	Outlet pressure	Gage pressure
Initial conditions	Pressure	101325 Pa

3.4.3. Mesh and Discretization

Since the domain is periodical, the fluent simulation domain can reduce the analysis only for one blade at a time (1/3 of the full model), then applying the periodic boundary conditions at 120° rotation will give us the torque and power results. The computational domain with the external fluid model is given in the next figures.

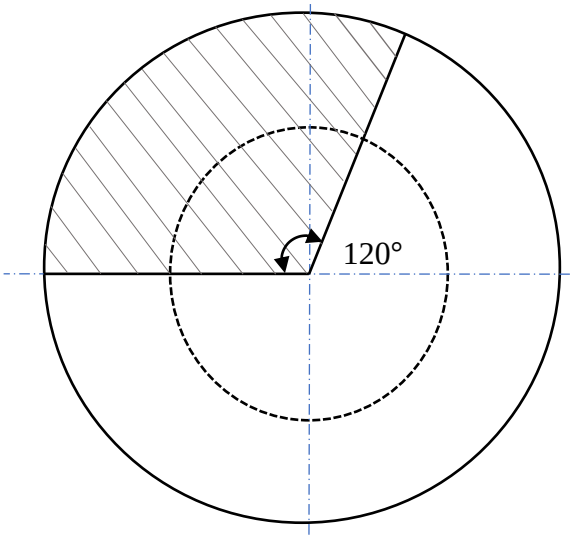

Figure 22: Periodically assumptions

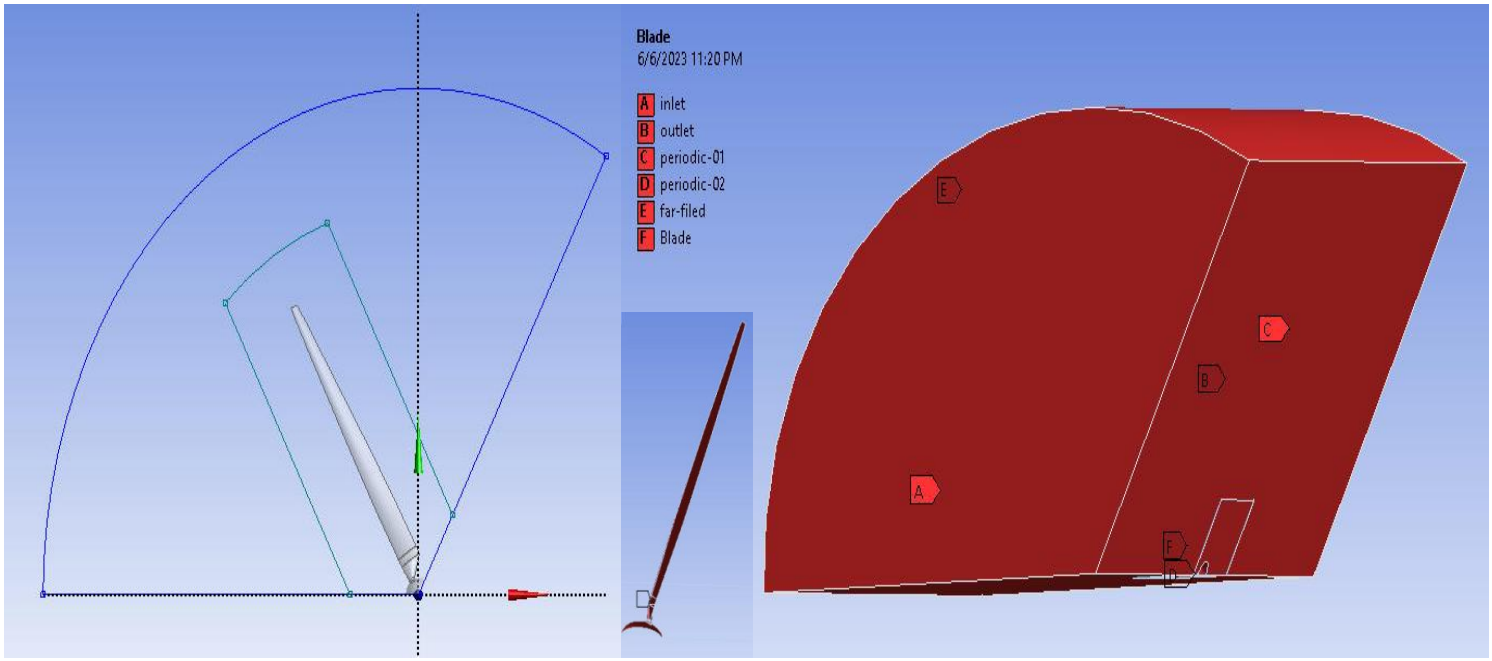

Figure 23: Blade Geometry with Fluid domain with a named selection

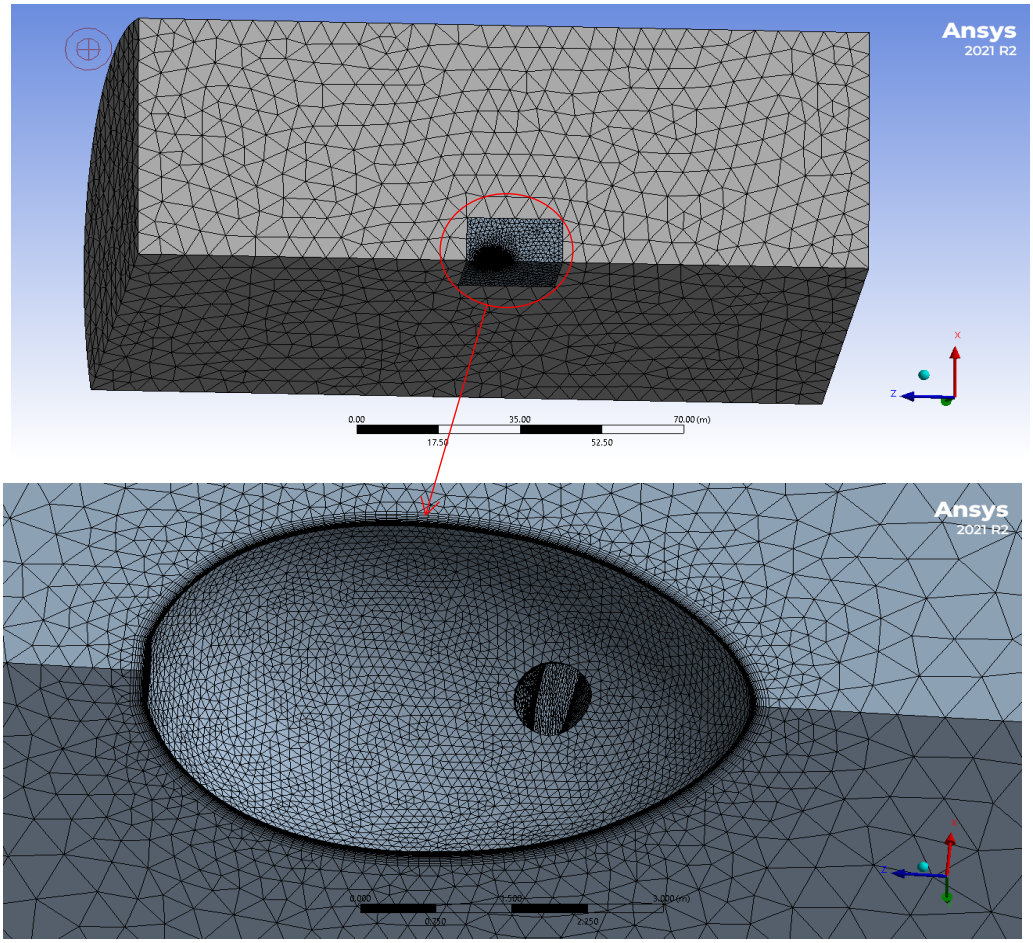

Figure 24: Tetrahedral mesh with several mesh elements in ANSYS Fluent 2021R2

While discretizing the computational geometry a fine tetrahedral cell was generated. Considering the mesh quality with minimum orthogonal quality > 0.1 or maximum skewness < 0.95 different mesh techniques are implemented on the blade geometry. Figure 24 shows the tetrahedral mesh with inflation on the blade surface the Mesh Matrix report indicates report the maximum skewness value is 0.64 which is less than 0.95 and the minimum orthogonal quality is 0.5 which is greater than 0.1. Generally, the maximum number of nodes generated from the generated mesh is 278,155 and the number of elements is 1,093,556.

3.2.1. Results and Discussion

The aerodynamic characteristics of the morphing wind turbine blade were investigated using ANSYS Fluent 2021R2 at different bending angles, the bending angles were (0°-20°).After checking the mesh quality again mesh optimization is done on ANSYS Fluent, by converting the tetrahedral mesh domain to polyhedral. The overall advantage of the polyhedral meshes over the tetrahedral meshes is it reduces the cell count. Researches show that polyhedral mesh lowers almost 3-5 times than the original unstructured tetrahedral mesh; hence this saves computational time and gives more realistic result compared with original unstructured tetrahedral mesh cells.

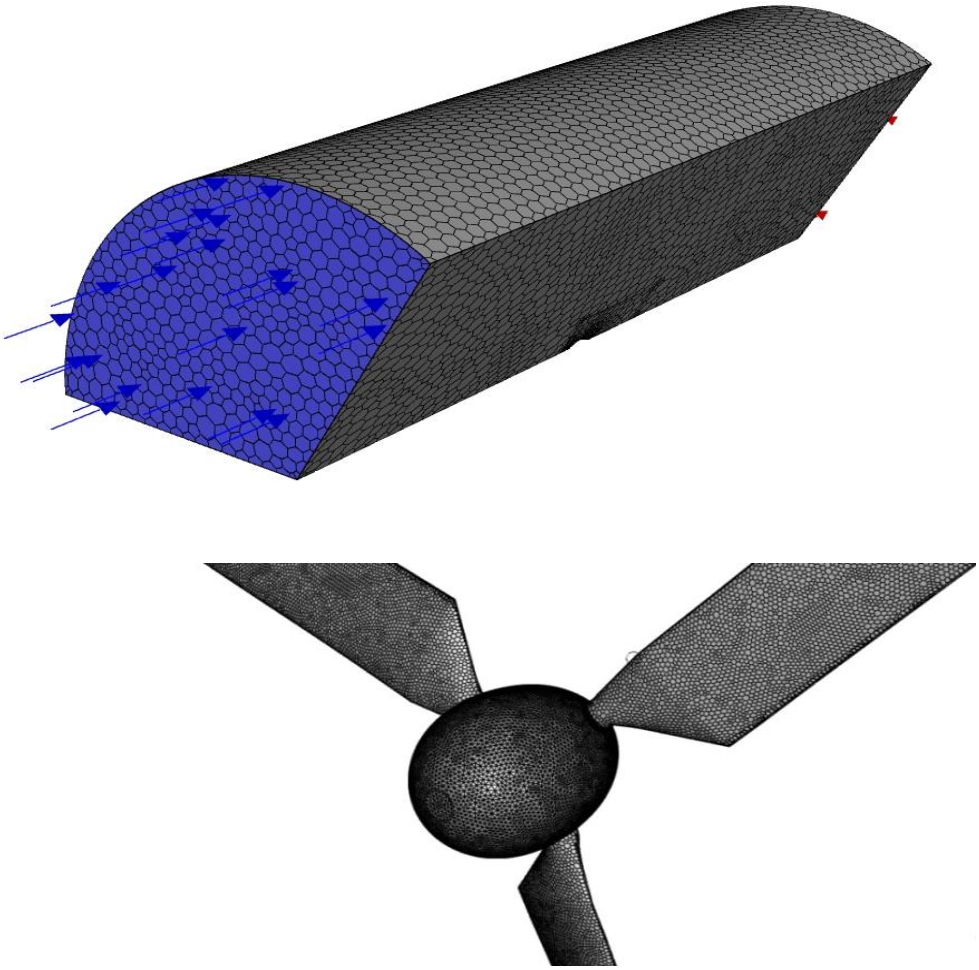

Figure 25: Polyhedral mesh domain in ANSYS Fluent 2021R2

Figure 25, shows the optimized polyhedral mesh domain, Herein the number of tetrahedral cells is reduced from 759127 to 173145 after converting to polyhedral mesh on ANSYS Fluent this indicates number if mesh cells is reduced about 4.5 times.

To address the economic advantage of morphing technologies in global rigid blade operational HAWT projects using life cycle comparative analysis with assumed Rayleigh distribution on next chapter, a conventional SANY SE7715 wind turbine [44] installed in the Adama II wind farm project with the same operating conditions and partial design specifications was taken as a reference site. As per A. Debru [38] investigation the annual mean wind speed of the reference site as is 7.75 m/s. Likewise the rated wind speed of the reference wind turbine (SANY SE7715) installed in Adama II project is 11.5 m/s. Therefore the simulation results in this paper is based on the annual mean and rated inlet velocity boundary conditions. The first one Fig. (26-29) is based on annual mean wind speed (7.75 m/s) of the reference site Adama II wind farm project. Whereas the second one Fig. (30-33) is based on rated wind speed (11.5 m/s) of the reference site. Based the analytical calculation results the maximum tip speed at the annual mean, and rated wind speeds are 54.25 m/s and 78.5 m/s respectively.

3.2.1.1. SIMULATION RESULTS AT ANNUAL AVERAGE WIND SPEED

The Frist CFD simulation results Fig. (26-29), are velocity contour plots at annul mean wind speed 7.75 m/s of reference site.

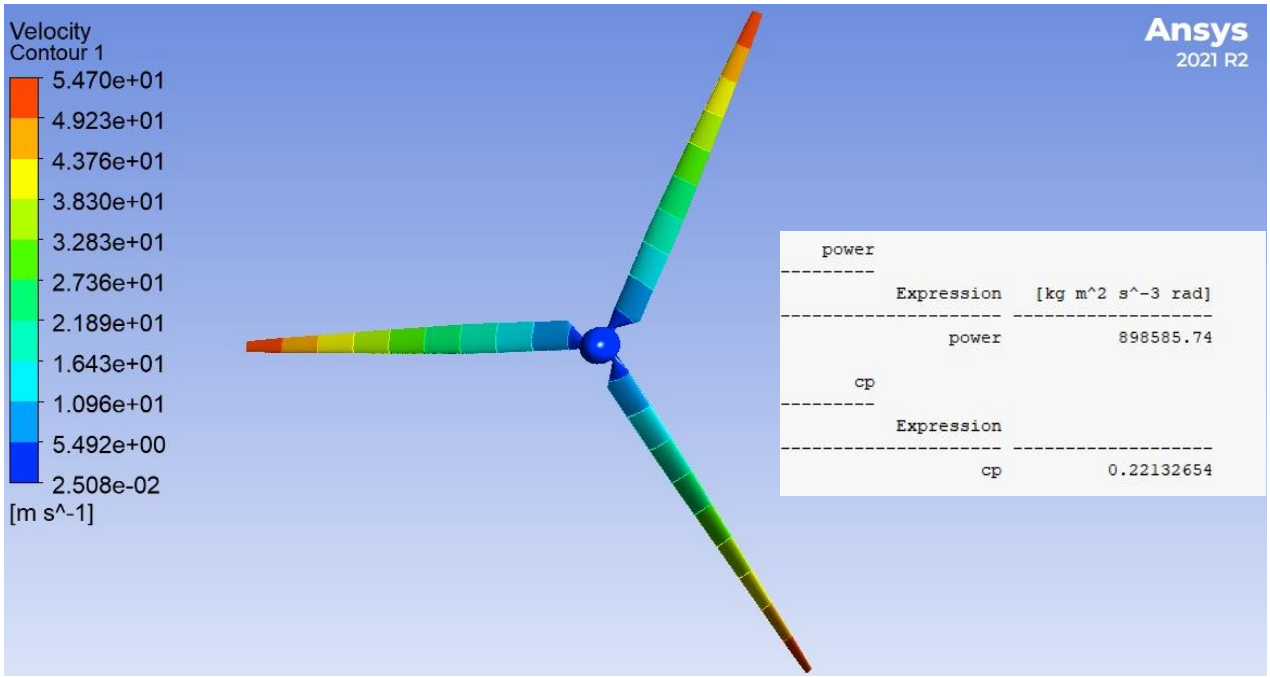

Figure 26: Velocity contour results at 0° bending angle and inlet velocity 7.75 m/s

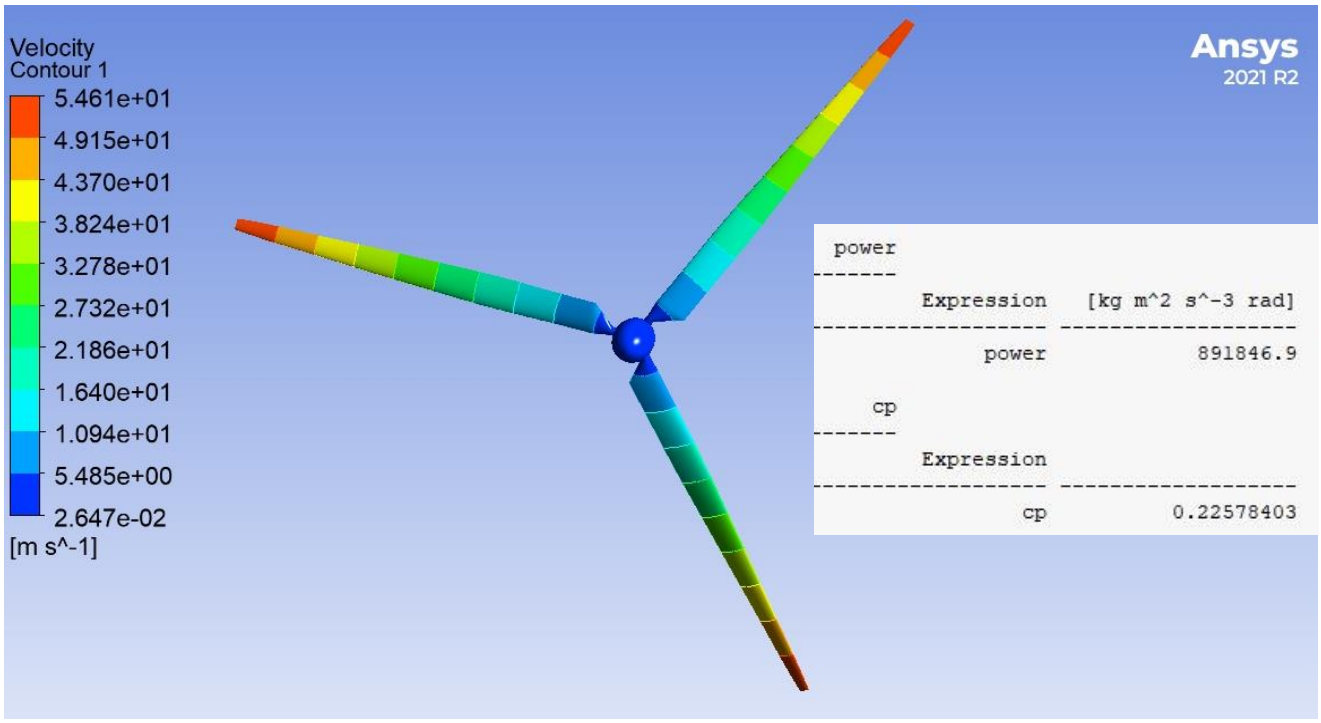

Figure 27:Velocity contour results at 10° bending angle and inlet velocity 7.75 m/s

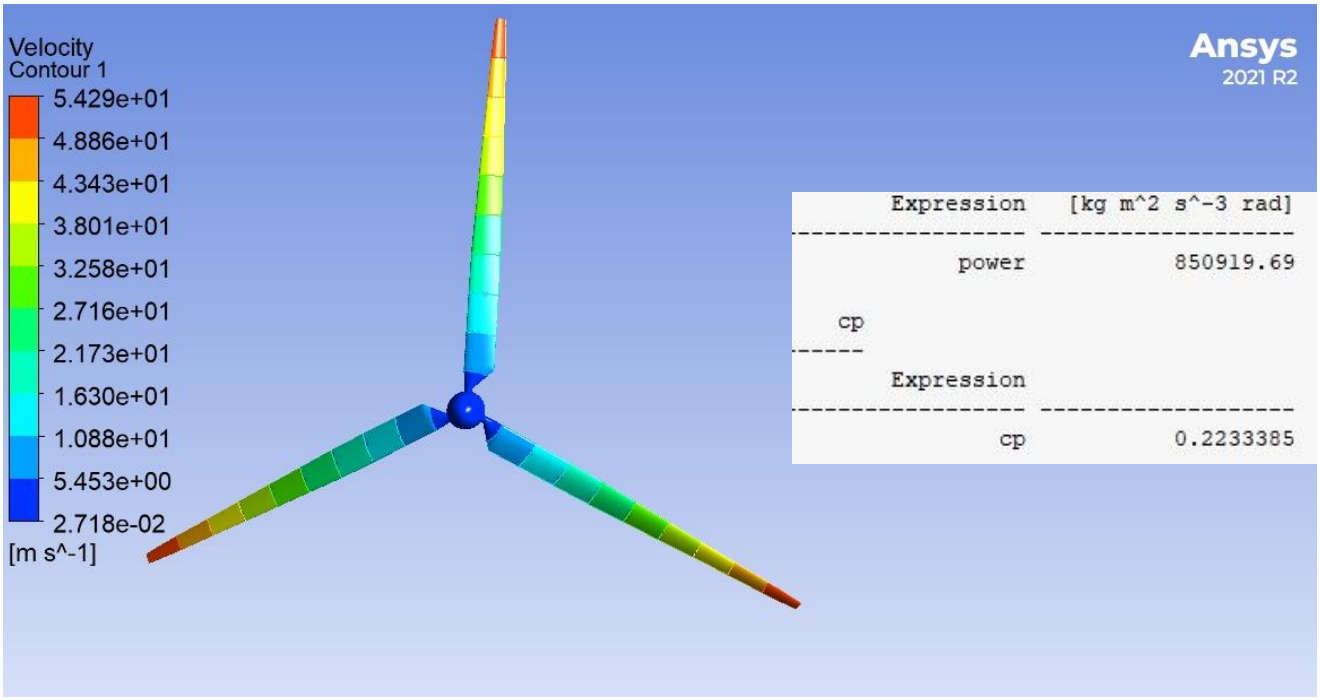

Figure 28: Velocity contour results at 15° bending angle and inlet velocity 7.75 m/s

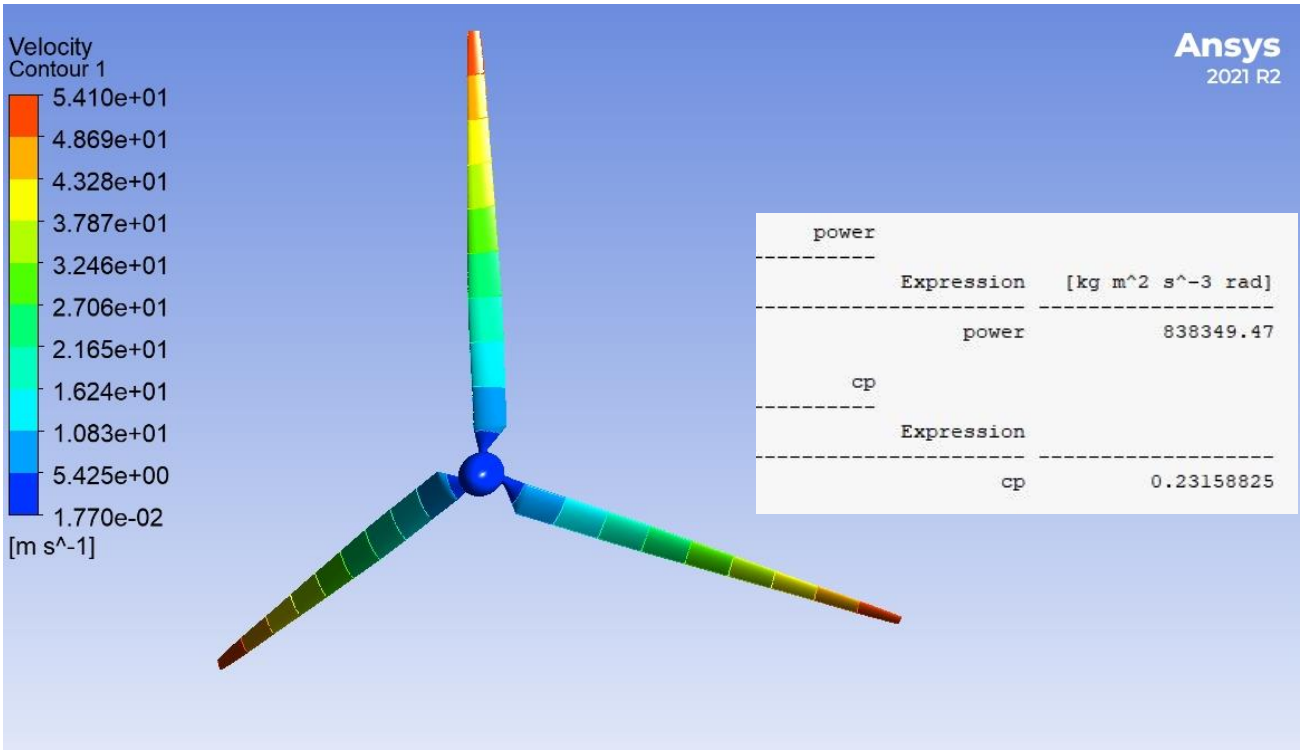

Figure 29: Velocity contour results at 20° bending angle and inlet velocity 7.75 m/s

- Figure 26 ,shows the CFD results at 0° bending angle of power, Tip Speed (V_{Tip}), and power coefficient (C_p) with values of 891846.90 W, 54.7 m/s, and 0.221 respectively.
- Figure 27, shows the CFD results at a 10° bending angle of power, Tip Speed (V_{Tip}), and power coefficient (C_p) with values of 898585.90 W, 54.6 m/s, and 0.225 respectively.
- Figure 28, shows the CFD results at a 15° bending angle of power, Tip Speed (V_{Tip}), and power coefficient (C_p) with values of 850919.69 W, 54.29 m/s, and 0.223 respectively.
- Figure 29, shows the CFD results at 20° bending angle of power, Tip Speed (V_{Tip}), and power-coefficient (C_p) with values of 838349.70 W, 54.10 m/s, and 0.23 respectively.

From the simulation results the average power produced when the blades swings from (0-20) degree bending angle keeping the tip speed at the given inlet velocity is 870 KW.

3.2.1.2. SIMULATION RESULTS AT RATED WIND SPEED

Figure (30-33), shows the CFD simulation results of velocity contour plots with maximum tip speed, produced power, and power-coefficient (C_p) results at rated speed 11.5 m/s inlet velocity.

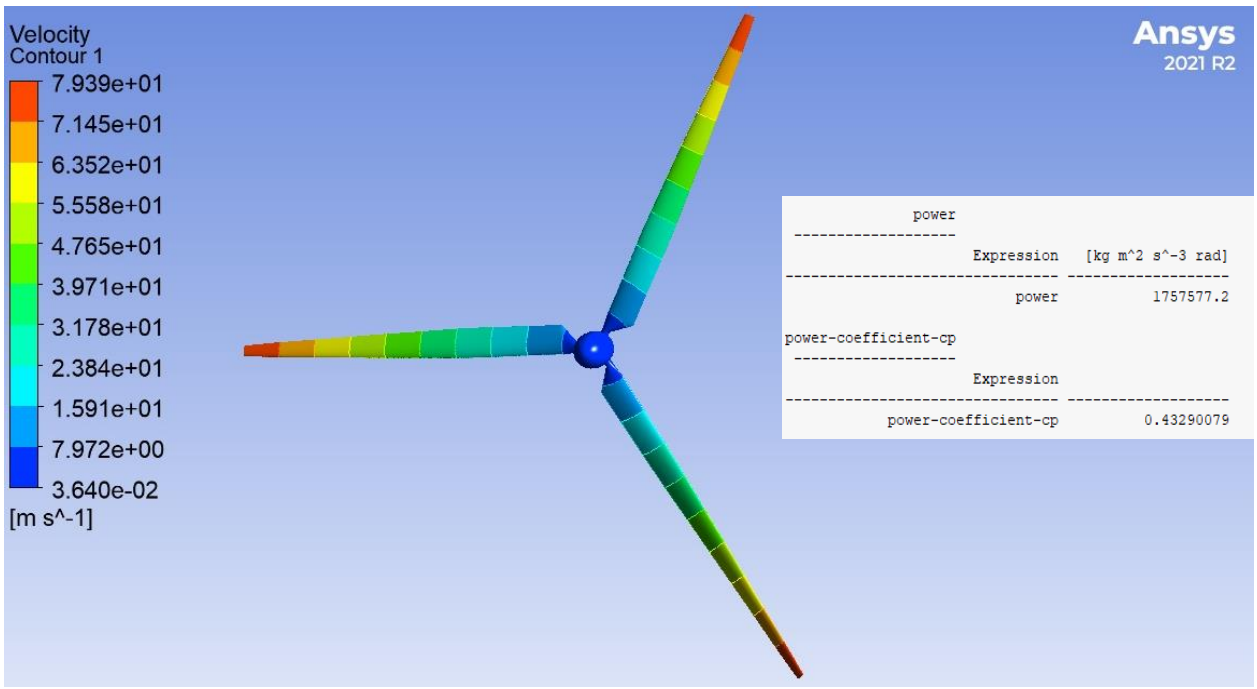

Figure 30: Velocity contour results at 0° bending angle, and inlet velocity 11.5 m/s

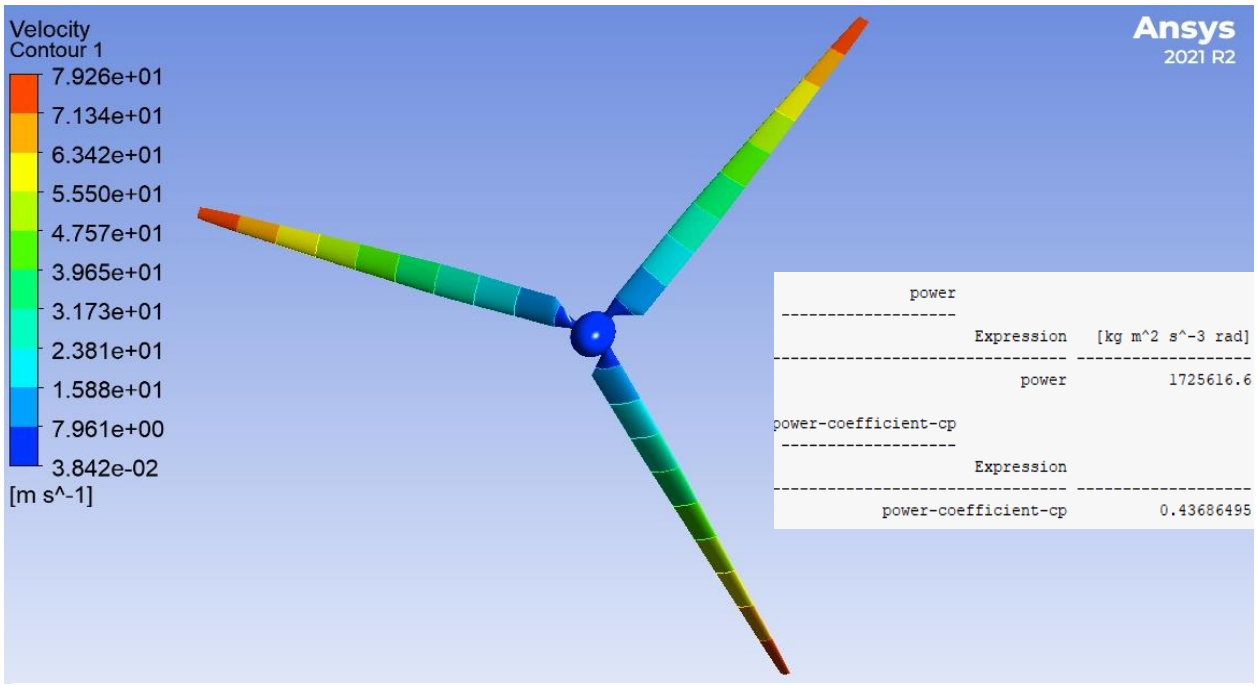

Figure 31: Velocity contour results at 10° bending angle, and inlet velocity 11.5 m/s

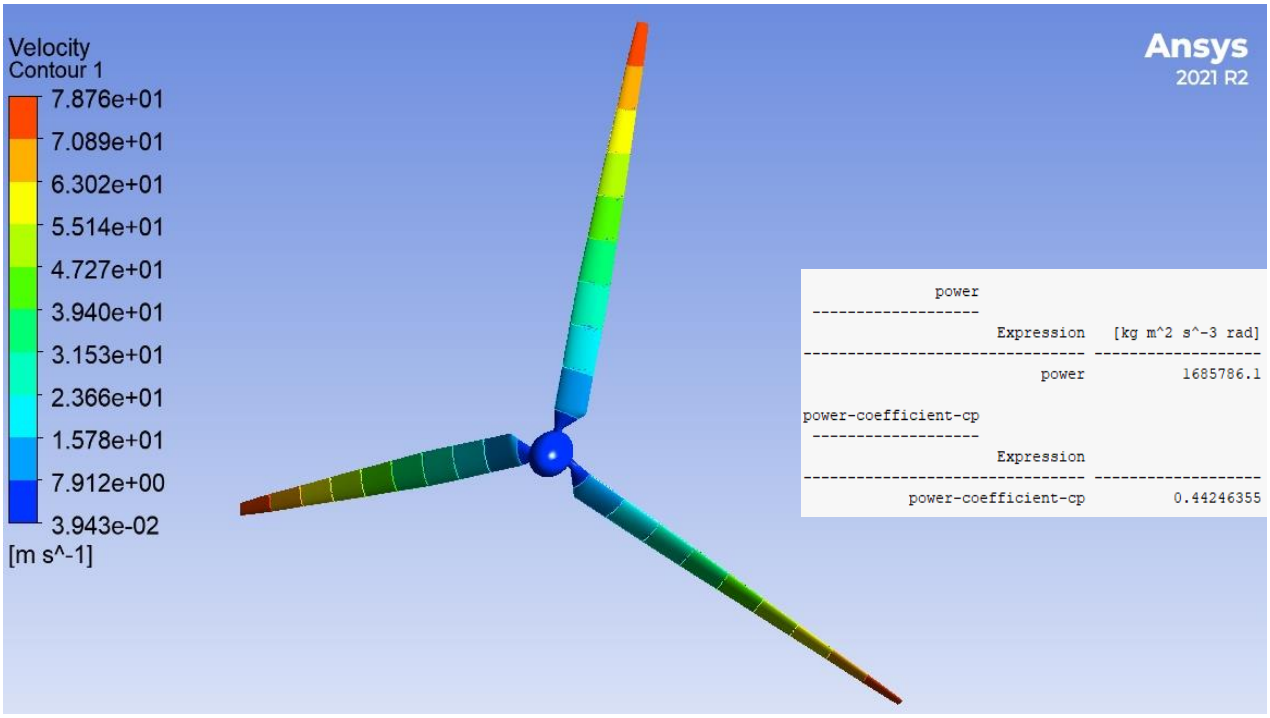

Figure 32：Velocity contour results at 15° bending angle, and inlet velocity 11.5 m/s

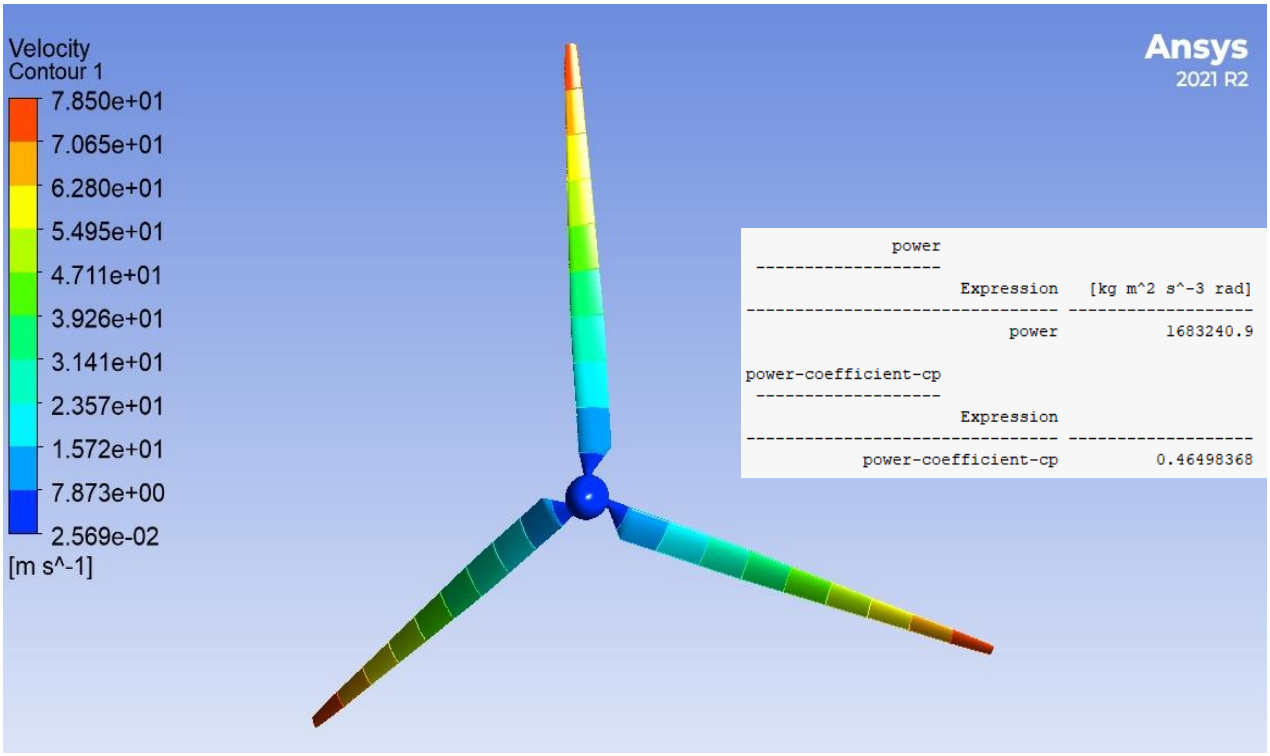

Figure 33：Velocity contour results at 20° bending angle, and inlet velocity 11.5 m/s

- Figure 30, shows the CFD results at 0° bending angle of power, Tip Speed (V_{Tip}), and power coefficient (C_p) with values of 1757577.2 W, 79.39 m/s, and 0.4329 respectively.
- Figure 31, shows the CFD results at a 10° bending angle of power, Tip Speed (V_{Tip}), and power coefficient (C_p) with values of 1725616.6 W, 79.26 m/s, and 0.4368 respectively.
- Figure 32, shows the CFD results at a 15° bending angle of power, Tip Speed (V_{Tip}), and power coefficient (C_p) with values of 1685786.1 W, 78.76 m/s, and 0.442 respectively.
- Figure 33, shows the CFD results at 20° bending angle of power, Tip Speed (V_{Tip}), and power-coefficient (C_p) with values of 1683240.9 W, 78.50 m/s, and 0.465 respectively.

The basic assumptions of the above simulations scenario were based on the blade design at the rated wind speed with a specified bending angle should allow a maximum tip speed ratio. However as seen from the above simulation result Fig. (30-33), the maximum tip speed is almost equivalent to the assumed value, in addition, the simulation result shows as the bending angle increases the power coefficient increase and the power generated slightly decreases as the power is directly proportional to the swept area and the tip velocity also decreases while the swept area is reduced. As a result at higher wind speeds this novel design approach will work by maximizing the power efficiency with twist bending augmented system.

In this section, the value obtained from the CFD simulation results will be compared with the theoretical calculation results. However, to measure the strength and direction of the linear relationship between the theoretical (anaytical), and CFD simulation results of the design parameters, Mintab software with Pearson's correlation method is used. According to Pearson's correlation method principle to study two variables of x & y, Pearson's correlation coefficient (r-value) can be calculated using the following formula.

$$r = \frac{n\left(\sum xy\right) - \left(\sum x\right)\left(\sum y\right)}{\left[n\sum x^2 - \left(\sum x\right)^2\right]\left[n\sum y^2 - \left(\sum y\right)^2\right]} \quad \text{.....(3.23)}$$

Where "n" is the number of samples, and x and y are the design parameters such as power, Tip speed, and power coefficient (Cp) calculated using both theoretical and CFD simulations results. The correlation coefficient between 0.8 to 1.0 is a very strong correlation. Table 12, shows the summary results of both the theoretical and CFD simulation Results.

Table 12: Comparison of results at rated wind speed

Bending angle	Theoretical (analytical) results			CFD simulation results		
	Rated Power	Power coefficient (C_p)	Tip Speed (V_{Tip})	Power (W)	Power coefficient (C_p)	Tip Speed (V_{Tip})
0°	1.8 MW	0.42	78.75 m/s	1757577.2	0.433	79.39 m/s
10°		0.43		1725616.6	0.437	79.26 m/s
15°		0.45		1685786.1	0.442	78.76 m/s
20°		0.47		1683240.9	0.465	78.50 m/s

Using Mintab software the correlation between the theoretical and CFD simulation results is evaluated, hence the Pearson's correlation coefficient (r-value) results of power produced, Power coefficient, and Tip Speed (V_{Tip}) are 0.957, 0.943, and 0.978 respectively. The R-value shows a very strong correlation between the theoretical and CFD simulation results. According to this correlation result it can be concluded that the power produced, Power coefficient (C_p), and Tip Speed (V_{Tip}) of the CFD simulation results of the proposed novel design is perfectly matched with the theoretical results.

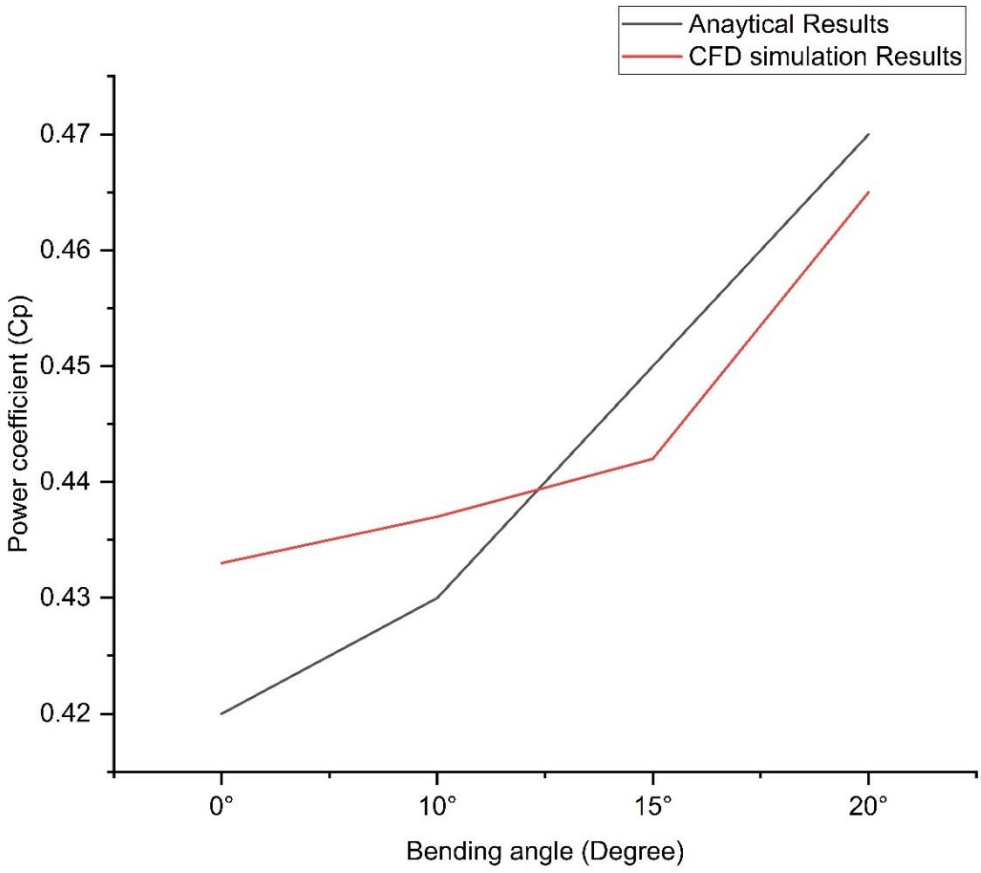

Figure 34: Theoretical vs CFD simulations results of power coefficient (Cp)

To observe the significat power improvement graphically, it is also possible to draw the approximated power curve with respect to the reference SANY7715 wind turbine power curve [45] and the CFD simulation results of the newly introduced morphing blade design. A power curve one of the basic charactersitcs of wind turbine, shows the relationship between wind speed at the loaction of the turbine, and the expected power being produced. To ensure the wind turbine performs as per the spesfication this graph is manadtory for the wind turbine manufactures. As seen on next Fig.35, the SANY 1.5 MW WTG's power curve is drawn in one graph, the blue line is the graph for the SANY SE7715 wind turbine installed in Adama II wind farm project, taken as a reference site from the comparative analysis.

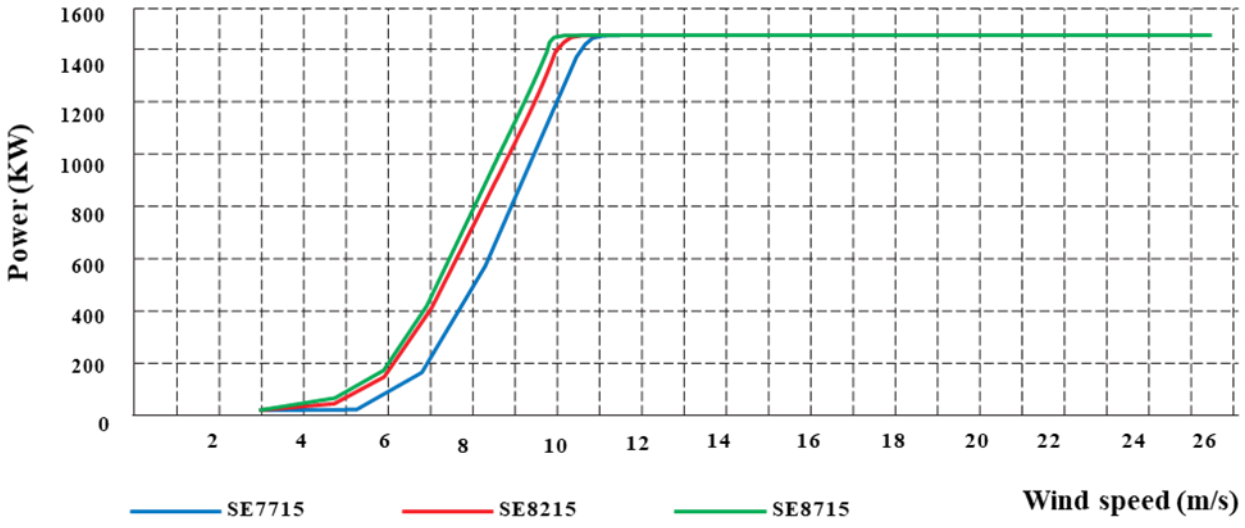

Figure 35: SANY 1.5 MW WTG's Power Curves [35]

For wind farm expansion and improvement, precise model of power curve is an important tool to forecast the power produced accurately. However using the avilable data, power curve of the refernce SANY7715 wind turbine, and the CFD simulation results of the novel palm tree inspried morphing blade, the power curve for both design approches is precisely modeled in Fig.36. The morphing blade power curve is developed using non-parametric modeling, to find the relationship between the input wind speed and the power output on some points using interpolation technique

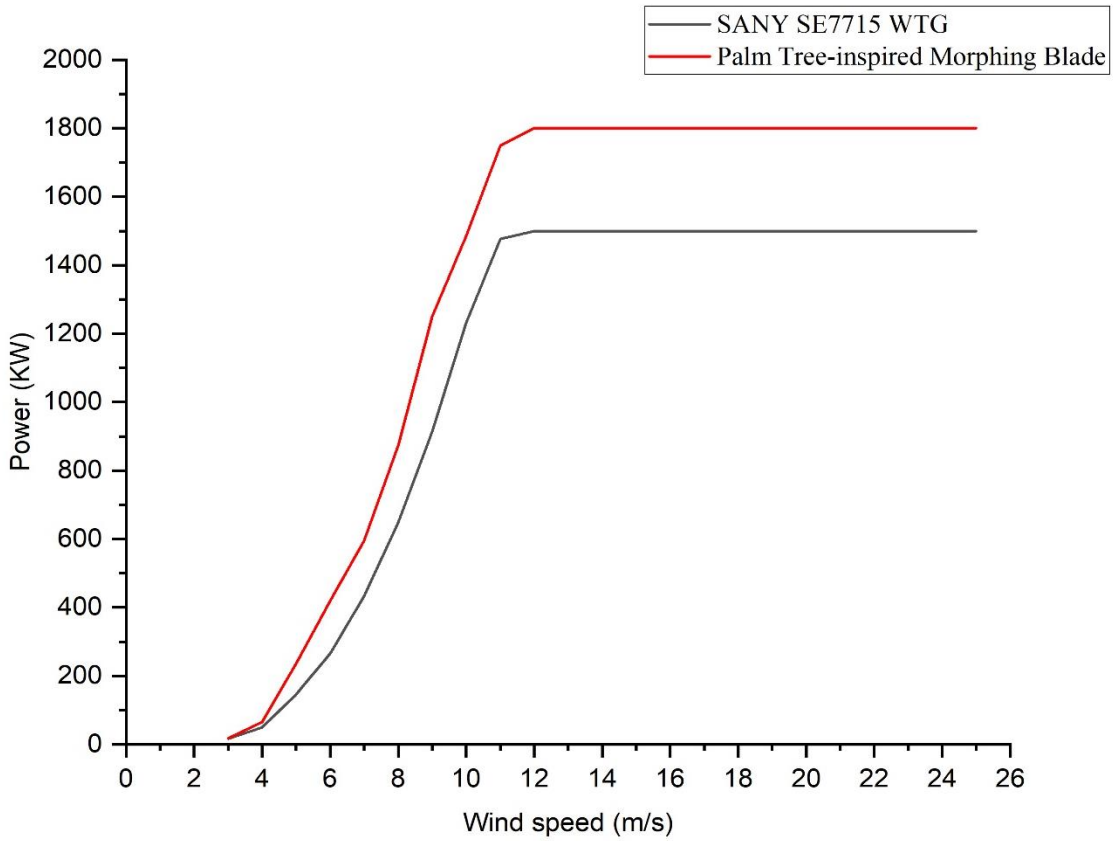

Figure 36: Power Curve Palm Tree-inspired Wind Turbine Blade Vs SANY SE7715 WTG

Figure 36, showes the power curve of palm tree-inspired wind turbine blade vs SANY SE7715 WTG.. As shown on the graph the power produced of the newly introduced morphing blade is significantly higher than the reference site at any point. The approximated rated power for the newly designed bio-inspired morphing blade is about 1.8 MW, whereas the conventional SANY SE7715 WTG is 1.5 MW. Therefore using palm tree inspired morphing wind turbine design approach, it is possible to increase the power produced of the wind turbine technology to the remarkable level.

Chapter Four: Life Cycle Analysis (LCA)

4.1. Conceptual framework of LCA

According to International Standards Organization (ISO) definition, life cycle analysis (LCA) is a stepwise approach to evaluate the products and process's environmental burden by identifying the energy, material used, and released wastes, which helps to implement better opportunities for improvement [26]. ISO 1400 series developed the general framework of the conceptual life cycle analysis (LCA) as shown below [26].

.

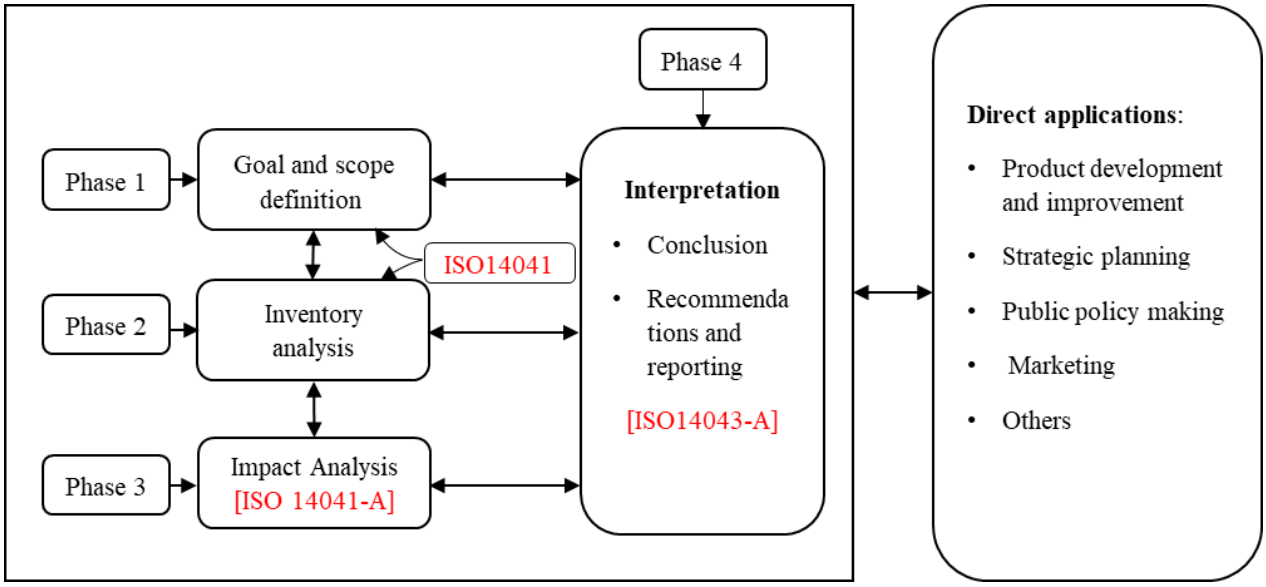

Figure 37: Conceptual general framework of LCA

In this paper, a bio-inspired novel design approach of a passively induced morphing blade with a twist-augmented bending system is introduced. The objective of this concept design is to improve the power efficiency and lifetime of the horizontal axis wind turbines. The blade material is carbon fiber and the design allows a higher Tip speed ratio (TSR) while the blade swings within the allowed range of bending angle. The rated power of the proposed wind turbine is 1.8 MW. The available rated wind speed, bending, and twist angles are the input variables, whereas the quantitative power produced and efficiency is the output data of this project. The knowledge-based compatibility analysis of the proposed morphing blade design needs further experimental investigation for better decisions on product development. In this paper, the scope of the life cycle assessment (LCA) for the proposed morphing blade design is limited to a comparative analysis of annual energy production with the reference conventional horizontal axis wind turbine blades. The direct application of this life cycle assessment is to put strategic planning for product development on the improved wind turbine technology.

4.2. Comparative Analysis of Annual Energy Production

Comparison of Annual Energy Production (AEP) on varies wind turbine technologies is the most important life cycle assessment in wind turbines, which helps to put conclusions and recommendations for further improvement [14, 38]. In this paper comparing the AEP of the newly introduced palm tree inspired morphing blade with the reference conventional wind turbine blades will be investigated in details. The AEP depends on the produced power and the probability of the available wind speed, Hence the wind speed can be modeled by using a Rayleigh Distribution. Average wind speed and shape factors (k) are the two parameters used to define the probability curve [14]. Therefore, the probability of the wind speed P (v) for a given average wind speed is calculated using the following formula [39].

$$P(v) = \frac{\pi}{2}\frac{v}{\bar{v}^2}\exp\left(-\frac{\pi}{4}\left(\frac{v}{\bar{v}}\right)^2\right) \quad \text{..... (4.1)}$$

Adama II wind farm project with SANY SE7715 wind turbines [44] is taken as reference to compare the AEP of the Novel palm tree inspired morphing blade introduced, while the partial design specifications and boundary conditions of the novel palm-tree inspired HAWT design, is the same with the Adama II wind farm project it is possible to compare the AEP at the same average annual wind speed. [38], have done detailed investigation on Adama II wind farm project "performance assessment compared with the feasibility study". Therefore the results obtained by those authors are used as secondary data's for the AEP compression purpose.

As per the researchers investigation the site's average annual wind speed at 70 m was 7.75 m/s and 2 years SCADA data were used for the energy performance evaluation, Finally the study shows the average AEP obtained for each turbine was around 5.588 GWh which is about 570 GWh gross annual energy production for the total 102 sets [38].

Using the above ANSYS Fluent software based analysis the power produced of the novel design at the reference site's annual mean wind speed is 870 KW, calculating the AEP of the newly introduced palm tree inspired morphing blade at annual mean wind speed gives 7.62 GWh/Year, which is around 36.4 % higher than Adama II wind farm project AEP production. Indeed it can be concluded that replacing the whole 102 sets of WTs with the newly introduced morphing ability wind turbines can give as around 776.95 GWh gross annual energy production, assuming 100% capacity factor for both cases.

Chapter Five: Conclusion and Future Work

A passively induced nature-inspired novel design approach from a palm tree is introduced to improve the power efficiency and lifetime of HAWTs as a concept design. In this novel design approach, the rotor speed is regulated by a twist-augmented bending system and the blade restoration at low wind speed is performed by a spring-augmented pivot hinge system.

To address systematically the intended objectives of this research project, a detailed methodology was followed. After conducting a literature review on wind turbine profiles, design techniques, and performance ranges, then the analytical modeling of the concept design is implemented. Due to its nearly flat surface, NACA 4412 Applicable profiles, and Carbon Fiber material were selected for the proposed morphing blade design. Based on the detailed design specification and modeling approaches a knowledge-based design compatibility analysis (DCA) was investigated, indeed the design is compatible. Then the 3D modeling at different bending angles was modeled using CERO PTC 8, and ANSYS Fluent 2021R2 was for the CFD analysis. Since the domain is periodical, the fluent simulation domain was used 1/3 of the full model, then the periodic boundary conditions at 120° rotation were applied. The computational analysis of the proposed morphing blade design is based on a simplified Reynolds Averaged Navier-Stokes (RANS) governing equation called Spalart-Allmaras (SA) turbulence model. From the CFD analysis report, the power produced at the reference site's annual mean wind speed of 7.75 m/s and rated inlet velocity of 11.5 m/s were obtained as 870 KW and 1712.781 KW respectively. To measure the strength and direction of the linear relationship between the theoretical and CFD simulation results, Minitab software with Pearson‟s correlation method was used, indeed the R-values of correlation results show a very strong correlation.

Under the life cycle analysis (LCA), a conventional SANY SE7715 wind turbine installed in the Adama II wind farm project was taken as a reference site to compare the Annual Energy production (AEP) with novel palm-tree inspired morphing blade design. Using software-based analysis the AEP of the newly introduced palm tree-inspired morphing blade at 7.75 m/s annual mean wind speed is 7.62 GWh/year, likewise, the average AEP of the reference site as per the prior researcher’s investigation is 5.59 GWh which is about 570 GWh gross annual energy production for the total 102 sets [27]. This indicates the AEP of the novel morphing ability wind turbine is 36.4 % higher than the Adama II wind farm project. Indeed it can be concluded that replacing the whole 102 sites of WTs with the newly introduced morphing ability wind turbines can achieve more than 36% power improvement which is around 776.95 GWh gross annual energy production. Assume a 100% capacity factor for both cases. From prior researchers’ investigation, using morphing blade technology, it is possible to improve the performance of wind turbines by up to 20% over

conventional wind turbine blades [6]. In this paper, the conventional SANY SE7715 wind turbines is improved by 36.4 % using the newly introduced palm tree-inspired wind turbine blade. To summarize the work, this remarkable efficiency improvement is obtained as the result of the following optimizations.

- The drag coefficient of the proposed MB design becomes lower as the bending angle increases.
- The proposed morphing blade design is a twist-augmented bending system, hence, the blade is twisted with an angle of (10-20) degrees throughout the cord length, with the ability to optimize the blade profile according to the direction of the wind load.
- The NACA 4412 airfoil profile used for this design is a nearly flat surface which prevents the negative ground effect that occurs with the extreme camber while this increase the power efficiency.
- The proposed morphing design allows a higher tip speed ratio, while the blade swings from (0-20) degrees depending on the wind speed to maximize the power efficiency.

Finally, the detailed design of the inner structures of the palm tree-inspired morphing blade, detailed structural load analysis, prototype, and experimental investigation are left as part of future work.

REFERENCE

[1] A. MUKTAR, "NOISE IMPACT ASSESSMENT OF ADAMA I WIND FARM," 2016.

[2] M. Stiebler, Wind energy systems for electric power generation. Springer Science & Business Media, 2008.

[3] C. Global, "GWEC| global wind report 2021," Global Wind Energy Council: Brussels, Belgium, 2021.

[4] P. J. Bradbury, P. X. Nguyen, C. R. Jenkins, and S. H. Frankel, "Axial flow fan having counter-rotating dual impeller blade arrangement," ed: Google Patents, 2003.

[5] D. W. MacPhee and A. Beyene, "Performance analysis of a small wind turbine equipped with flexible blades," Renewable Energy, vol. 132, pp. 497-508, 2019.

[6] K. Ishii, R. Adler, and P. Barkan, "Application of design compatibility analysis to simultaneous engineering," AI EDAM, vol. 2, no. 1, pp. 53-65, 1988.

[7] V. W. Tam, Y. Zhou, C. Illankoon, and K. N. Le, "A critical review on BIM and LCA integration using the ISO 14040 framework," Building and Environment, vol. 213, p. 108865, 2022.

[8] R. U. Maheswari and J. Tamilvendhan, "Analysis of modelling of active stall controlled and active pitch controlled variable speed wind turbines," International Journal of Modern Engineering Research, vol. 2, no. 4, pp. 2662-2667, 2012.

[9] D. G. Shepherd, "Historical development of the windmill," Cornell Univ., Ithaca, NY (USA). Dept. of Mechanical and Aerospace Engineering, 1990.

[10] M. M. Hasan, "Design and performance analysis of small scale horizontal axis wind turbine for nano grid application," 2017.

[11] V. Cognet, S. C. Du Pont, and B. Thiria, "Material optimization of flexible blades for wind turbines," Renewable Energy, vol. 160, pp. 1373-1384, 2020.

[12] D. W. MacPhee and A. Beyene, "Fluid–structure interaction analysis of a morphing vertical axis wind turbine," Journal of Fluids and Structures, vol. 60, pp. 143-159, 2016.

[13] A. Rathod, N. Raut, S. Patil, K. Kamble, and S. Shisode, "Aerodynamic Analysis of Morphing Blade for Horizontal Axis Wind Turbine," International Journal of Mechanical Engineering and Technology, vol. 8, no. 1, 2017.

[14] W. Wang, S. Caro, F. Bennis, and O. R. Salinas Mejia, "A simplified morphing blade for horizontal axis wind turbines," Journal of solar energy engineering, vol. 136, no. 1, 2014.

[15] N. None, "20% wind energy by 2030: Increasing wind energy's contribution to US electricity supply," EERE Publication and Product Library, Washington, DC (United States), 2008.

[16] R. Opie, "Pitch Control Critical for Wind Power," Machine Design, vol. 2, 2018.

[17] M. Puterbaugh and A. Beyene, "Parametric dependence of a morphing wind turbine blade on material elasticity," Energy, vol. 36, no. 1, pp. 466-474, 2011.

[18] P. Krawczyk, A. Beyene, and D. MacPhee, "Fluid structure interaction of a morphed wind turbine blade," International Journal of Energy Research, vol. 37, no. 14, pp. 1784-1793, 2013.

[19] T. Chuamvarasart, C. Chantharasenawong, and S. Wongkittirat, "Conceptual design of small wind turbine blades with morphing ability," 2014.

[20] M. S. Selig and B. D. McGranahan, "Wind tunnel aerodynamic tests of six airfoils for use on small wind turbines," J. Sol. Energy Eng., vol. 126, no. 4, pp. 986-1001, 2004.

[21] A. Beyene and D. Mangalekar, "Part-Load Performance of Twist-Coupled Flexible Turbine Blade at Low Reynolds Number," Proceedings of ECOS, 2009.

[22] D. W. MacPhee and A. Beyene, "Experimental and fluid structure interaction analysis of a morphing wind turbine rotor," Energy, vol. 90, pp. 1055-1065, 2015.

[23] L. Y. Pao and K. E. Johnson, "Control of wind turbines," IEEE Control systems magazine, vol. 31, no. 2, pp. 44-62, 2011.

[24] J. N. Sørensen, General momentum theory for horizontal axis wind turbines. Springer, 2016.

[25] V. Reyes, J. J. Rodríguez, O. Carranza, and R. Ortega, "Review of mathematical models of both the power coefficient and the torque coefficient in wind turbines," in 2015 IEEE 24th international symposium on industrial electronics (ISIE), 2015: IEEE, pp. 1458-1463.

[26] M. Yurdusev, R. Ata, and N. Çetin, "Assessment of optimum tip speed ratio in wind turbines using artificial neural networks," Energy, vol. 31, no. 12, pp. 2153-2161, 2006.

[27] M. Agrawal and G. Saxena, "Analysis of wings using airfoil NACA4412 at different angle of attack," IJMER, pp. 1467-1469, 2013.

[28] E. N. Jacobs, K. E. Ward, and R. M. Pinkerton, The Characteristics of 78 related airfoil section from tests in the Variable-Density Wind Tunnel (no. 460). US Government Printing Office, 1933.

[29] M. A. Hossain, M. N. Uddin, R. Mustak, and M. Mashud, "Experimental study of aerodynamic characteristics of airfoils using different shaped dimples," The International Journal Of Engineering And Science (IJES), vol. 4, no. 1, pp. 13-17, 2015.

[30] A. E. Ockfen and K. I. Matveev, "Aerodynamic characteristics of NACA 4412 airfoil section with flap in extreme ground effect," International Journal of Naval Architecture and Ocean Engineering, vol. 1, no. 1, pp. 1-12, 2009.

[31] L. Mishnaevsky Jr, K. Branner, H. N. Petersen, J. Beauson, M. McGugan, and B. F. Sørensen, "Materials for wind turbine blades: An overview," Materials, vol. 10, no. 11, p. 1285, 2017.

[32] B. L. Ennis et al., "Optimized carbon fiber composites in wind turbine blade design," Sandia National Lab.(SNL-NM), Albuquerque, NM (United States); Oak Ridge …, 2019.

[33] E. Möllerström, P. Gipe, J. Beurskens, and F. Ottermo, "A historical review of vertical axis wind turbines rated 100 kW and above," Renewable and Sustainable Energy Reviews, vol. 105, pp. 1-13, 2019.

[34] P. Bortolotti, A. Kapila, and C. L. Bottasso, "Comparison between upwind and downwind designs of a 10 MW wind turbine rotor," Wind Energy Science, vol. 4, no. 1, pp. 115-125, 2019.

[35] G. N. Abramovich, T. Girshovich, S. I. Krasheninnikov, A. Sekundov, and I. Smirnova, "The theory of turbulent jets," Moscow Izdatel Nauka, 1984.

[36] M. K. C. M. Chaudhary and S. Prakash, "Experimental Investigations of Small horizontal axis wind turbine rotors," Journal of Engineering Research, vol. 10, no. 3B, 2022.

[37] T. Graedel, "Streamline Life-Cycle Assessment Prentice Hall," Upper Sddle River, New Jersey, 1998.

[38] A. Debru, M. Bayray, and M. Molinas, "ADAMA-II wind farm performance assessment in comparison to feasibility study," Wind Engineering, vol. 46, no. 2, pp. 503-517, 2022.

[39] W. Wang, S. Caro, F. Bennis, and O. R. Salinas Mejia, "Optimal design of a simplified morphing blade for fixed-speed horizontal axis wind turbines," in International Design Engineering Technical Conferences and Computers and Information in Engineering Conference, 2012, vol. 45028: American Society of Mechanical Engineers, pp. 233-242.

[40] J. Jauregui, F. Herbert, and K. Castillo, "A Shape-Morphing Subsystem for Small Wind Energy Conversion Systems," in Turbo Expo: Power for Land, Sea, and Air, 2020, vol. 84249: American Society of Mechanical Engineers, p. V012T42A020.

[41] A. R. Ali, M. Z. Akhter, and F. K. Omar, "Performance enhancement of a small-scale wind turbine featuring morphed trailing edge," Sustainable Energy Technologies and Assessments, vol. 46, p. 101229, 2021.

[42] T. N. Santelo, C. M. R. de Oliveira, C. D. Maciel, and J. R. B. de A. Monteiro, "Wind Turbine Failures Review and Trends," Journal of Control, Automation and Electrical Systems, pp. 1-17, 2022.

[43] NREL: 'Statistics show bearing problems cause the majority of wind turbine gearbox failures', 2015. U.S. Department of Energy & National Renewable Energy Laboratory (NREL). Available from: http://energy.gov/eere/wind/articles/statistics-show-bearingproblems-cause-majority-wind-turbine-gearbox-failures, accessed 7 January 2016.

[44] SANY Group Co., Ltd. SANY SE7715 wind turbine, https://en.wind-turbine-models.com/turbines/2080-sany-se7715, www.sanygroup.com,

APPENDIX

Table 4. NACA 4412 database coordinates [Source: UIUC airfoil coordinates database]

NACA4412 Coordinates					
Top coordinates			Bottom coordinates		
X	Y	Z	X	Y	Z
0	0	0	0	0	0
0.0125	0.0244	0	0.0125	-0.0143	0
0.025	0.0339	0	0.025	-0.0195	0
0.05	0.0473	0	0.05	-0.0249	0
0.075	0.0576	0	0.075	-0.0274	0
0.1	0.0659	0	0.1	-0.0286	0
0.15	0.0789	0	0.15	-0.0288	0
0.2	0.088	0	0.2	-0.0274	0
0.25	0.0941	0	0.25	-0.025	0
0.3	0.0976	0	0.3	-0.0226	0
0.4	0.098	0	0.4	-0.018	0
0.5	0.0919	0	0.5	-0.014	0
0.6	0.0814	0	0.6	-0.01	0
0.7	0.0669	0	0.7	-0.0065	0
0.8	0.0489	0	0.8	-0.0039	0
0.9	0.0271	0	0.9	-0.0022	0
0.95	0.0147	0	0.95	-0.0016	0
1	0.0013	0	1	-0.0013	0

NACA 4412 profile

Table 5. Published technical data for Zoltek Px35 Carbon Fiber properties

Zoltek Px35 Carbon Fiber Properties	
Material Properties	Value
Tensile strength	4.137 MPa
Yield strength	267 m/kg
Tensile Modulus	242 GPa
Electrical Resistivity	0.00155 ohm-cm
Density	1.82 g/cc
Fiber diameter	7.2 microns
Carbon content	95%